Dynamic regulation of mRNA acetylation at synapses by spatial memory in mouse hippocampus

Hai-Qian Zhou[1,2#], Zhen Zhu[1#], Jia-Wei Zhang[1#], Wei-Peng Lin[1,3,4], Hao-JY Jin[1], Yang-Yang Ding[1], Shuai Liu[1,3*] and Dong-Min Yin[1,3,5*]

[1]Key Laboratory of Brain Functional Genomics, Ministry of Education and Shanghai, Affiliated Mental Health Center, School of Life Science, East China Normal University, Shanghai, 200062, China

[2]Department of Neurology, Shanghai Fifth People's Hospital, Fudan University, Shanghai, 200240, China.

[3]Shanghai Changning Mental Health Center, Affiliated Mental Health Center of East China Normal University, Shanghai, 200335, China

[4]Chongqing Key Laboratory of Precision Optics, Chongqing Institute of East China Normal University, Chongqing, 401120, China

[5]NYU-ECNU Institute of Brain and Cognitive Science at NYU Shanghai, Shanghai, 200062, China

[#]H-Q Z, Z Z and J-W Z contributed equally to this work.

[*]Correspondence should be addressed to

Prof. Shuai Liu,

Email: sliu@psy.ecnu.edu.cn

or

Prof. Dong-Min Yin,

Email: dmyin@brain.ecnu.edu.cn

Abstract

Precise regulation of protein synthesis is critical for brain functions such as long-term memory, and its dysregulation is implicated in numerous memory disorders. While mRNA methylation such as N6-methyladenosine (m6A) that has been widely studied in memory, the role of mRNA acetylation remains largely unknown. N4-acetylcytidine (ac4C), the only known form of RNA acetylation in eukaryotes, promotes mRNA stability and translation. In this study, we identified the ac4C epitranscriptome in mouse hippocampal homogenates and synaptosomes through ac4C-RNA immunoprecipitation followed by next-generation sequencing (acRIP-seq). The Morris water maze (MWM) was employed to induce and evaluate memory acquisition and forgetting processes. We show that synaptic ac4C levels are dynamically regulated, increasing after memory formation and returning to baseline after natural forgetting. The dynamic changes of ac4C-mRNAs regulated by memory were validated by ac4C dot-blot, liquid chromatography-tandem mass spectrometry (LC-MS/MS), and acRIP-qPCR analysis. We further demonstrate that NAT10, the ac4C writer, in mouse hippocampus is important for spatial memory via regulating memory-related mRNAs, proteins, and ultimately synaptic plasticity. Lastly, we generated a freely-accessible website (http://ac4catlas.com) that included the dataset of ac4C epitranscriptome in mouse hippocampus. Altogether these results demonstrate that dynamic and localized mRNA acetylation is important for synaptic plasticity and memory.

Introduction

Spatiotemporal regulation of protein synthesis is essential for brain functions, particularly learning and memory[1,2]. For instance, local protein synthesis near stimulated synapses plays critical roles in synaptic plasticity and memory consolidation[3,4]. Mechanistically, epigenetic regulations on DNA and histone proteins have been widely studied in the context of learning and memory[5,6]. However, the roles of chemical modifications on mRNA in learning and memory have only become appreciated in recent years[7-9]. Especially, N6-methyladenosine (m6A), a well-studied form of mRNA methylation has been shown to regulate synaptic plasticity as well as learning and memory[10-12].

N4-acetylcytidine (ac4C) is the only known form of RNA acetylation in eukaryotes[13]. Initially, ac4C was identified in the transfer RNA (tRNA) anticodon[14-17]. Later studies revealed that ac4C also occurred in the 18S ribosomal RNA (rRNA)[18]. More recently, ac4C has been found in mRNA from mammalian cells, where it was reported to promote mRNA stability and translational efficiency[19,20]. N-acetyltransferase 10 (NAT10) is the only known ac4C writer in mammalian cells[21]. NAT10-mediated mRNA acetylation has been reported to regulate tumorigenesis[22,23], stem cell differentiation[24], cardiac remodeling[25], germ cell maturation[26] and pain signaling in the spinal cord[27,28]. However, the function and regulatory mechanisms of mRNA acetylation in the brain remain poorly understood.

The hippocampus plays an important role in learning and memory[29]. Pyramidal neurons in the CA3 region of hippocampus establish direct projection to CA1 pyramidal neurons through the Schaffer collateral (SC) pathway, known as the SC-CA1 synapse. The glutamatergic transmission at SC-CA1 synapses was found to be enhanced following training in the Morris water maze (MWM)[30], a behavioral paradigm for learning and memory[31]. Long-term potentiation (LTP), a widely-studied form of synaptic plasticity in hippocampus, is most closely linked to learning and memory[32]. Several studies showed that mRNAs and ribosomes were present in the synaptosomes, contributing to protein synthesis at synapses[33]. In principle, neural activities can

regulate local protein synthesis through post-transcriptional modification of synaptic mRNAs[34]. However, whether synaptic mRNAs are subjected to NAT10-mediated acetylation and whether this process contributes to synaptic plasticity and memory remain elusive.

In this study, we conducted ac4C dot-blots, liquid chromatography-tandem mass spectrometry (LC-MS/MS) and acRIP-seq to study the ac4C modification of mRNA in mouse hippocampus during and after training in the MWM. We found that ac4C modification of mRNA was increased in the synaptosomes (SYN), rather than in the homogenates (HOM), following memory, and subsequently returned to baseline after memory forgetting. We further demonstrate that NAT10, the ac4C writer, in mouse hippocampus is important for memory through regulating memory-related mRNAs, proteins and ultimately synaptic plasticity. Collectively these results demonstrate the importance of mRNA acetylation in memory. The dataset of ac4C epitranscriptome from mouse hippocampus is freely accessible at the website (http://ac4catlas.com/).

Results

Presence of ac4C modification of polyA RNA in mouse hippocampus

Recent studies raised the debate about the presence of ac4C mRNA from mammalian cells[35,36]. We first investigate whether ac4C is a detectable modification of mRNA from mouse hippocampus. To this end, we purified polyadenylated (polyA) RNA from HOM of mouse hippocampus and determine their ac4C levels using LC-MS/MS. The purity of polyA RNA was verified by bioanalyzer analysis (Figure 1A and 1B) and dramatic reduction of 18S rRNA relative to total RNA in the analysis of reverse transcription followed by quantitative PCR (RT-qPCR) (Figure 1C). An ac4C standard curve was generated to calculate the stoichiometry levels of ac4C in polyA RNA samples. Both the ac4C (or C) and m6A (or A) peaks can be detected by the chromatograms in the standard samples but not in the blank solution (Figure 1D-G). The polyA RNA purified from the HOM of mouse hippocampus showed ac4C peaks with a stoichiometry level of 0.426 ± 0.049% (n = 3 biological replicates) (Figure 1H). Likewise, the polyA RNA

88 purified from the HOM of mouse hippocampus showed m6A peaks with a
89 stoichiometry level of 0.223 ± 0.046% (n = 3 biological replicates) (Figure 1I), which
90 is consistent with the previous study from mouse brain[37]. When the polyA RNA samples
91 were incubated with 50 mM NH_2OH for 1 h before LC-MS/MS, a protocol of chemical
92 deacetylation[38], the stoichiometry levels of ac4C were significantly reduced (Figure
93 1H), indicating the validity of the LC-MS/MS analysis. By contrast, the stoichiometry
94 levels of m6A in polyA RNA samples remained unchanged after NH_2OH treatment
95 (Figure 1I), supporting the specificity of the deacetylation protocol. Altogether these
96 results demonstrate the presence of ac4C modification in polyA RNA from mouse
97 hippocampus. Given that polyA RNA consists of mRNA and long noncoding RNA
98 (lncRNA)[39], we further performed acRIP-seq to analyze the ac4C mRNA in mouse
99 hippocampus.

100 **Characterization of ac4C mRNA in the HOM of mouse hippocampus after**
101 **memory**

102 We used the behavioral protocol of MWM[40] to study how memory regulate mRNA
103 acetylation in mouse hippocampus. The control mice were placed in the MWM with a
104 visible platform once a day for 2 days, and thus could reach the visible platform in the
105 target region without training (Figures S1A and S1B). However, the control mice could
106 not remember the target region during the probe test at day 6 (Figures S1A and S1C).
107 In contrast, the memory mice were subjected to training in the MWM with a hidden
108 platform (Figures S1D and S1E). The memory mice took 5 days of training to remember
109 the target region during the probe test at day 6 (i.e., post-training day 1) (Figures S1E
110 and S1F), indicative of memory. Consistent with the previous study[41], the memory mice
111 could not remember the target region during the probe test at day 20 after staying in the
112 home cages for 2 weeks (i.e., post-training day 15) (Figures S1D and S1G), indicating
113 that memories were naturally forgotten (Figure S1H).

114 We next performed acRIP-seq[19] to identify ac4C mRNA in the HOM of mouse
115 hippocampus. Two libraries of RNA (acRIP and input) were subjected to the next-
116 generation sequencing (NGS) for each sample (Table S1). The acRIP-seq reads were

mapped to mouse hippocampal transcriptome to identify ac4C enriched regions relative to input, and the fold enrichment (FE) of an ac4C peak was defined as acRIP / input (Figure S2A). An ac4C peak was considered positive when its FE > 2 and adjusted p-values < 0.05[42].

We performed acRIP-seq for three HOM replicates from control and memory mice one hour after probe tests in the MWM (i.e., at day 6). The ac4C peaks and ac4C mRNAs identified in three biological replicates of control and memory mice were largely overlapped (Figures S2B and S2C). These results indicate the consistency of the acRIP-seq for mouse hippocampus. The ac4C peak that were identified from at least two of the three biological replicates were considered reliable. Only mRNAs corresponding to these reliable ac4C peaks are defined as reliably ac4C mRNAs. We identified 14516 ac4C peaks and 8303 ac4C mRNAs from the HOM of control mice (Figure S2B and Table S2), and 13348 ac4C peaks and 8107 ac4C mRNAs from the HOM of memory mice (Figures S2C and Table S2). Moreover, the acRIP-seq revealed the same consensus motif AGCAGCTG in the ac4C peak regions from three biological replicates of control and memory mice (Figure S2D).

When we compared the transcripts with ac4C modifications to the entire transcriptome, we found that 54.1 ± 2.62% (n = 3 biological replicates) of the mRNAs in the mouse hippocampus were modified by ac4C. In line with the previous study from HeLa cells[19], metagene profile analysis revealed that most ac4C peaks were located within the coding sequence (CDS) of mRNAs in mouse hippocampus, with lower density in the 5' and 3' untranslated regions (Figures S2E and S2F). To further assess the reproducibility of our ac4C detection, we performed Upset plot analysis which revealed 4,494 peaks common to all three biological replicates in control mice and 4,110 peaks in memory mice (Figures S2G and S2H). The numbers of ac4C peak per acetylated mRNA were comparable across three biological replicates and between control and memory mice (Figure S2I). Likewise, the ac4C dot-blots of polyA RNA, and the cumulative distribution of ac4C mRNAs in the HOM were similar between the control and memory mice (Figures S2J and S2K). The cumulative distribution of

146 mRNA counts in the HOM that were revealed by the NGS of input RNA were also
147 similar between control and memory mice (Figure S2L). Altogether these results
148 suggest that the total levels of ac4C mRNA in the HOM of mouse hippocampus may
149 not be altered by memory.

150 **Dynamic change of ac4C polyA RNA in the SYN of mouse hippocampus during**
151 **memory**

152 We next purified the SYN fraction from mouse hippocampus, enriched for synaptic
153 proteins (PSD95 and synapsin 1) and depleted of cytoplasm (the S2 fraction)-restricted
154 protein (α-tubulin) (Figure 2A). We then analyzed the levels of ac4C polyA RNA
155 purified from the SYN with the ac4C dot-blots. The control and memory mice at day 1
156 (i.e., training phase day 1 for memory mice) showed similar levels of ac4C polyA RNA
157 in the SYN (Figure 2B). Strikingly, the levels of ac4C polyA RNA showed a significant
158 increase in the SYN of memory mice at day 6, compared with controls (Figure 2C).
159 However, the levels of ac4C polyA RNA returned to control levels in the SYN of
160 memory mice at day 20 (Figure 2D). These results suggest that acetylation of polyA
161 RNA was upregulated in the SYN of mouse hippocampus after memory formation
162 memory but returned to control levels after memory forgetting. The dynamic change of
163 ac4C RNA in the SYN of mouse hippocampus during memory was verified by the assay
164 of LC-MS/MS (Figure 2E).

165 **Characterization of ac4C mRNA in the SYN of mouse hippocampus**

166 Given that the amount of RNA that could be purified from SYN (200 ng per mouse
167 hippocampus) is much less than that from HOM (50 μg per mouse hippocampus), we
168 used the protocol of low-input acRIP-seq to identify ac4C mRNAs in the SYN (see
169 details in the Methods). Due to the limited yield of SYN RNA, we purified the SYN
170 RNA from the hippocampus of 10 adult mice and combined them into one sample. Six
171 total samples from control and memory mice at days 1, 6, and 20 were subjected to low-
172 input acRIP-seq. Two libraries (acRIP and input) were sequenced for each sample
173 (Table S1). To increase the data reliability for low-input acRIP-seq, transcripts that were
174 identified in our own sequencing and at least two of the three synaptosome databases[43-

175 [45] were considered reliable and included in the analysis.

176 The transcripts and ac4C mRNAs identified from the SYN of control and memory
177 mice at days 1, 6 and 20 were largely overlapped (Figures S3A-B and S3E-F; Table S3).
178 We found that 58.61 ± 1.39% of the mRNAs in the SYN from control mouse
179 hippocampus were modified by ac4C. On average, every acetylated transcript had 1.77
180 ± 0.05 ac4C peaks in the SYN from control mouse hippocampus. Moreover, the low-
181 input acRIP-seq revealed the same consensus motif AGCAGCTG in the ac4C peak
182 regions of SYN mRNA from control and memory mice at days 1, 6 and 20 (Figure S3C
183 and S3G). In line with the results from HOM, most ac4C peaks were identified in CDS
184 of SYN mRNA from both control and memory mice (Figures S3D and S3H). These
185 results indicate the consistency of the low-input acRIP-seq for SYN mRNA.

186 **Dynamic change of ac4C mRNA in the SYN of mouse hippocampus during**
187 **memory**

188 The cumulative distribution of ac4C mRNAs in the SYN did not differ between control
189 and memory mice at day 1 (Figure 2F). In contrast, the cumulative distribution curve
190 of ac4C mRNAs in the SYN of memory mice had a significant rightward shift at day 6,
191 compared with control mice (Figure 2G). Intriguingly, the cumulative distribution of
192 ac4C mRNAs in the SYN of memory mice became indistinguishable from that of
193 control mice at day 20 (Figure 2H). The cumulative distribution of mRNA counts in the
194 SYN were similar between control and memory mice at days 1, 6, and 20 (Figures 2I-
195 2K). These results suggest that acetylation of mRNA rather than the total levels of
196 mRNA was increased in the SYN after memory, and mRNA acetylation returned to
197 control levels after memory forgetting, supporting the dynamic change of acetylation
198 of polyA RNA in the SYN during memory (Figures 2B-2E).

199 To further validate the distinct molecular characteristics of the "memory-day6"
200 group, we performed principal component analysis (PCA) based on global ac4C
201 modification profiles. The first two principal components accounted for 38% and 26%
202 of the total variance, respectively. The "memory-day6" samples clustered distinctly
203 from the other five groups, confirming a unique epitranscriptomic signature associated

with memory (Figures S3I). To identify the memory-induced synaptic ac4C (MISA) mRNA, we analyzed the fold change (FC) of ac4C mRNA in the SYN of memory versus control mice (L/C) at days 1, 6, 20 (Figures S3J-S3L). Here we analyzed the FE of all ac4C peaks to better reflect the acetylation level of individual mRNA. Acetylation of MISA mRNA should be upregulated after memory and return to control levels after memory forgetting. In other words, the ac4C of MISA mRNA should be upregulated specifically at day 6 (the cutoff value of upregulation is FC > 2) but not at days 1 or 20. Per these criteria, we identified 1237 MISA mRNAs whose ac4C levels were increased at day 6 rather than at days 1 or 20 in memory mice, compared with controls (Figure S3M; Table S4). In contrast, the transcription levels of MISA mRNAs were similar at days 1, 6, and 20 between control and memory mice (Figure S3M; Table S4).

A representative MISA mRNA for Arc

Gene ontology (GO) analysis indicated that MISA mRNAs were significantly enriched in the biological processes (BP) related with synaptic plasticity and learning or memory (Figure 3A; Table S4). Protein-protein interaction (PPI) network analysis of MISA mRNAs involved in learning or memory revealed several core genes such as activity-regulated cytoskeleton associated protein (Arc), glutamate receptor NMDA type subunit 1 (Grin1), and presenilin 1 (Psen1) (Figures 3A and 3B). ARC protein can be transported into dendrites and translated near activated postsynaptic sites after neural activities[46,47]. Different from other immediately early genes (IEG), Arc underwent repetitive cycles of transcription and local translation, which is critical for memory consolidation[48,49]. Although Arc is a promising "master regulator" of protein synthesis-dependent forms of memory, the mechanisms underlying the regulation of local translation of Arc in the SYN remained to be elucidated[50]. Analysis of the acRIP-seq data indicate that memory mice have elevated ac4C Arc mRNA in the SYN at day 6 rather than days 1 or 20, and similar levels of ac4C Arc mRNA in the HOM at day 6, compared with control mice (Figure 3C). The genome browser tracks for the ac4C of all MISA mRNAs were accessible at the ac4C website (http://ac4catlas.com/) to show altered ac4C in the SYN, and similar lack of change for those same RNAs in the HOM

233 at day 6.

234 Next, we used an orthogonal method to verify the dynamic change of ac4C Arc
235 mRNA in the SYN during memory. To this end, performed RT-qPCR analysis for Arc
236 mRNA from the input and acRIP samples from the SYN. The levels of input and acRIP-
237 Arc mRNA were similar in the SYN of control and memory mice at days 1 and 20
238 (Figures 3D, 3E, 3G and 3H). Likewise, the protein levels of ARC were also comparable
239 in the SYN of control and memory mice at days 1 and 20 (Figures 3F and 3I). Although
240 the levels of input Arc mRNA were not altered in the SYN of memory mice at day 6
241 (Figure 3J), the levels of acRIP-Arc mRNA and ARC proteins were significantly
242 increased in the SYN of memory mice at day 6, compared with controls (Figures 3K
243 and 3L). In contrast, the levels of Arc mRNA and ARC proteins were similar in the
244 HOM of control and memory mice at day 6 (Figures 3M and 3N). Note that Arc mRNA
245 levels in the IgG-IP samples were much lower than that in the acRIP samples (Figures
246 3E, 3H and 3K), indicating the specificity of RT-qPCR for acetylated Arc mRNA.
247 Altogether the results demonstrate that acetylation of Arc mRNA is specifically
248 increased in the SYN after memory but returned to control levels after memory
249 forgetting.

250 **Expression of Nat10 in the mature neurons of mouse hippocampus**

251 NAT10 is the only known ac4C writer[21]. Since the commercially available NAT10
252 antibodies were not suitable for immunostaining in the hippocampal slices, we used the
253 strategy of genetic labeling[51,52] to investigate the expression pattern of Nat10. To this
254 end, a heterozygous knockin mouse line ($Nat10^{Cre/+}$) that expressed the Cre
255 recombinase right after the start codon (ATG) of Nat10 gene was generated using the
256 CRISPR/Cas9 techniques (see details in the Method). Since the Cre recombinase and
257 Nat10 share the same regulatory elements for gene expression in the $Nat10^{Cre/+}$ mice,
258 the Nat10 expression pattern can be revealed through the Cre-reporting adeno-
259 associated virus (AAV) that express EGFP in a Cre-dependent manner. In this way, the
260 Nat10-positive cells would express EGFP in the Nat10 reporter mice (Figure 4A).

261 The dorsal hippocampus integrates multiple synaptic inputs from other brain

262 regions, and is critical for learning and memory[53-55]. To study the expression pattern of
263 Nat10 in the dorsal hippocampus of adult mice, we injected Cre-reporting AAV into the
264 dorsal hippocampus of 7-week-old Nat10$^{Cre/+}$ mice, and the fluorescent protein EGFP
265 was analyzed 3 weeks after AAV injection. Analysis of the EGFP-positive cells revealed
266 that Nat10 was mainly expressed in the pyramidal cell layer (sp) of CA1 region and
267 granule cell layer (gcl) of dentate gyrus (DG) (Figure 4B). Around 80% of Nat10-
268 expressing cells are mature neurons, evidenced by the overlay between EGFP and NeuN,
269 a protein marker for mature neurons (Figures 4C and 4D). Note that about 20% of
270 Nat10-positive cells are non-neuronal and probably glia cells. Moreover, about 75% of
271 Nat10-positive cells are excitatory pyramidal neurons in the CA1 region of mouse
272 hippocampus, indicated by the co-localization of EGFP with Neurogranin (NG), a
273 protein marker for excitatory pyramidal neurons (Figures 4C and 4E).

274 To validate the expression pattern of Nat10, we observed Cre signals in the
275 Nat10$^{Cre/+}$ mice using immunofluorescence. We found that most of the Cre-positive
276 cells were mature neurons within the CA1 region, with a small subset being GFAP-
277 positive astrocytes (Figure 4F-H). Collectively, these results indicate that Nat10 is
278 mainly expressed in mature neurons, with limited expression in glia cells.

279 **Increase of NAT10 proteins in the SYN after memory**

280 The above-mentioned data showed that the levels of ac4C mRNA were increased in the
281 SYN of mouse hippocampus after memory. Next, we aim to investigate whether the
282 protein levels of NAT10, the only known ac4C writer[21], are also regulated by memory.
283 Toward this aim, we purified the SYN fraction from the hippocampus of control and
284 memory mice at days 1, 6 and 20, and analyzed the protein levels of NAT10 by western
285 blots (Figure 5A). The protein levels of NAT10 in the SYN were similar between
286 control and memory mice at day 1 (Figure 5B). Interestingly, the protein levels of
287 NAT10 were significantly increased in the SYN of memory mice at day 6 (Figure 5C),
288 but returned to control levels at day 20 (Figure 5D). These results indicate that protein
289 levels of NAT10 are increased in the SYN after memory but return to normal levels
290 after memory forgetting (Figure 5E).

291 The protein levels of NAT10 were not altered in HOM of memory mice at day 6,
292 compared to controls (Figure 5F), suggesting that memory did not upregulate the de
293 novo protein synthesis of NAT10 in mouse hippocampus. To further explore the
294 distribution of NAT10 proteins in other subcellular fractions, we purified the nucleus
295 (N), cytoplasm (S2) and post-synaptic density (PSD) fractions from the hippocampus
296 of control and memory mice at day 6, and analyzed the protein levels of NAT10 in
297 different subcellular fractions (Figure 5G). The nuclear fraction was enriched for
298 histone but was depleted of cytoplasmic protein α-tubulin or synaptic protein SYN1
299 and PSD95, and vice versa for the S2 and PSD fractions (Figure 5H). The protein levels
300 of NAT10 in the nucleus did not change at day 6 after memory (Figure 5I). Strikingly,
301 the NAT10 proteins were significantly reduced in the cytoplasm (S2 fraction) but
302 increased in the PSD fraction at day 6 after memory (Figures 5J and 5K). These results
303 suggest that NAT10 proteins might be relocated from the cytoplasm to synapses in
304 mouse hippocampus after memory.

305 NAT10 belongs to the p300/CBP-associated factor (PCAF) subfamily of protein
306 acetyltransferase[56]. Next, we aim to investigate whether memory changed protein levels
307 of PCAF in the subcellular fractions of mouse hippocampus. The protein levels of
308 PCAF did not change in the nucleus, cytoplasm or PSD fractions of memory mice at
309 day 6, compared to controls (Figures 5L-5N), indicating that memory may not alter the
310 subcellular distribution of PCAF.

311 Next, we performed immunofluorescent staining to study the synaptic distribution
312 of NAT10 proteins in cultured hippocampal neurons with chemical LTP (cLTP)
313 stimulation (Figure S4A) – a cellular model of learning and memory[57,58]. In control
314 neurons treated with vehicle, NAT10 was mainly expressed in the nucleus and
315 cytoplasm (Figure S4B), which is consistent with the results of western blots (Figures
316 5I and 5J). However, 60 minutes after cLTP stimulation, the colocalization of NAT10
317 with PSD95, a protein marker for PSD fraction, was significantly increased, compared
318 with control neurons (Figures S4C and S4D). These results corroborate the in vivo
319 findings to demonstrate the increase of NAT10 proteins at synapses by neural activities.

Induction of ac4C modification of Arc by cLTP in hippocampal slices

Given our observation that cLTP stimulation promotes the redistribution of NAT10 protein to the postsynaptic density, we further examine the effects of cLTP stimulation on the ac4C levels of Arc, a typical MISA mRNA (Figure 3). The local translation of Arc at synapses is known to be activated by neural activities and important for LTP consolidation[59]. We employed acRIP-qPCR to analyze the ac4C levels of Arc mRNA in mouse hippocampal slices after cLTP stimulation. The results indicated that ac4C modifications of Arc mRNA in the synaptosomes were significantly increased (after being normalized by transcription levels) 1 h after cLTP stimulation compared with controls (Figures S4E and S4F), which is accompanied by the increase of Arc proteins in the synaptosomes after cLTP stimulation (Figure S4G). Together with the in vivo findings these data suggest that neural activities can upregulate ac4C modification of Arc mRNA at synapses.

NAT10-dependent ac4C polyA RNA in mouse hippocampus

To demonstrate the NAT10-dependent ac4C modification of poly A RNA, we used the Cre/Loxp strategy[60] to downregulate Nat10 expression in adult mouse hippocampus through injection of AAV-EGFP-P2A-Cre into the hippocampus of Nat10$^{flox/flox}$ mice. Given that Nat10 is mainly expressed in the mature neurons (Figure 4), the expression of EGFP-2A-Cre in the AAV was driven by the human synapsin 1 (Syn1) promoter, a neuron-specific promoter[61]. The Nat10$^{flox/flox}$ mice injected with AAV-EGFP and AAV-EGFP-P2A-Cre were named control and Nat10 conditional knockout (cKO) mice hereafter. Both the control and Nat10 cKO mice received stereotaxic AAV injection into the dorsal hippocampus, and the HOM of dorsal hippocampus were collected for biochemical assay 3 weeks after AAV injection (Figure S5A).

The fluorescent protein EGFP was expressed mainly in the CA1-3 regions and DG of mouse hippocampus 3 weeks after AAV injection (Figure S5B), indicating the successful infection of AAV. The protein levels of NAT10 were significantly reduced in the hippocampus of Nat10 cKO mice, compared with controls (Figures S5C and S5D), verifying the effective knockdown of NAT10 by the Cre/Loxp strategy. NAT10 was

349 previously described as a protein acetyltransferase against α-tubulin and histones[62,63].
350 However, immunoblotting with acetylation-specific antibodies showed no significant
351 change of protein acetylation in Nat10 cKO hippocampus, compared to controls
352 (Figures S5C, S5E and S5F). These results suggest the redundancy of acetyltransferases
353 for α-tubulin and histones in mouse hippocampus. In contrast, the ac4C modification
354 of polyA RNA was significantly decreased in the hippocampus of Nat10 cKO mice,
355 compared with controls (Figures S5G and S5H). As a control experiment,
356 downregulation of NAT10 did not affect the m6A modification of polyA RNA (Figures
357 S5I and S5J). The LC-MS/MS analysis of polyA RNA indicated that the stoichiometry
358 levels of ac4C rather than m6A were significantly reduced in the hippocampus of Nat10
359 cKO mice, compared with controls (Figures S5K and S5L). The partial reduction of
360 ac4C in the Nat10 cKO mice might be due to the limited infection areas of Cre-AAV,
361 or the Nat10 expression in non-neuronal cells, or the presence of other unknown ac4C
362 writers. Nonetheless, these results demonstrate that NAT10 specifically regulates ac4C
363 rather than m6A modification of polyA RNA in mouse hippocampus.

364 **NAT10-dependent ac4C mapping of SYN mRNA in memory mice**

365 Given that memory increased ac4C mRNA specifically in the SYN, we next aim to
366 identify NAT10-dependent ac4C modification of synaptic mRNAs. To this end, we
367 performed low-input acRIP-seq for SYN RNA purified from the hippocampus of
368 control and Nat10 cKO mice at day 6 after memory (Figure S6A). Due to the limited
369 yield of SYN RNA, we purified SYN RNA from the hippocampus of 10 mice and
370 combined them into one sample. Two biological samples from control and Nat10 cKO
371 mice at day 6 were subjected to low-input acRIP-seq to demonstrate the NAT10-
372 dependent ac4C modification of SYN mRNA. Two libraries (acRIP and input) were
373 sequenced for each biological sample (Table S3).

374 We identified 7097 and 1933 ac4C peaks from the SYN of control and Nat10 cKO
375 mice, respectively (Figure S6B). These results suggest a reduction of the ac4C peak
376 number by knockout of Nat10 in mature neurons of adult mouse hippocampus. Out of
377 7097 ac4C peaks identified in control mice, 6331 peaks were abolished and 408 peaks

378 were downregulated in Nat10 cKO mice, and these ac4C peaks were named NAT10-
379 dependent synaptic ac4C (NASA) peaks (Figure S6C) which were mainly localized in
380 the CDS region of mRNA (Figure S6D)

381 The Nat10 cKO mice also showed a reduction of ac4C mRNA number in the SYN,
382 compared with controls (Figure S6E). In contrast, the number of mRNA in the SYN
383 was similar between control and Nat10 cKO mice (Figure S6F). Likewise, the levels of
384 ac4C mRNA rather than total mRNA were significantly reduced in the SYN of Nat10
385 cKO mice, compared with controls, evidenced by the leftward-shifted cumulative
386 distribution curve of FE of ac4C mRNA in the Nat10 cKO mice (Figures 6A-6C). Out
387 of 3,778 ac4C-modified mRNAs identified in the SYN of control mice, 2,507 were
388 classified as diminished, indicating that their ac4C enrichment fell below the detection
389 threshold or became undetectable in Nat10 cKO mice (FE < 1 or peak lost). An
390 additional 839 mRNAs were downregulated, defined as showing significantly reduced
391 but still detectable ac4C levels in cKO mice compared to controls. Collectively, these
392 transcripts were referred to as NASA mRNAs (Figure S6G; Table S5). Analysis of the
393 overlap between MISA and NASA indicated that 717 out of 1237 MISA mRNAs were
394 regulated by NAT10 (Figure 6D).

395 To further investigate the molecular basis underlying the differential regulation of
396 MISA mRNAs by NAT10, we performed sequence motif analysis on the two distinct
397 gene populations - 717 NAT10-dependent MISA mRNAs (present in both MISA and
398 NASA populations) and 520 NAT10-independent MISA mRNAs (present only in MISA
399 but absent in NASA) (Figure 6D). Remarkably, these two gene sets exhibited distinct
400 ac4C consensus motifs (Figure 6D). The NAT10-dependent MISA mRNAs, displayed
401 the canonical AGCAGCTG motif that was consistently observed throughout our study.
402 In contrast, the NAT10-independent MISA mRNAs showed a fundamentally different
403 motif pattern, characterized by RGGGCACTAACY sequence. The complete
404 divergence in motif sequences between these two populations suggests that the NAT10-
405 independent MISA mRNAs may be regulated by as yet unidentified ac4C writers.

406 We next analyzed the cellular expression pattern of NASA mRNAs through the

407 single-cell RNA-seq atlas of mouse hippocampus (dropviz.org)[64]. The results indicated
408 that the expression of NASA mRNAs was mostly enriched in excitatory neurons (Figure
409 S6H), which is in line with the cellular expression pattern of NAT10 in mouse
410 hippocampus (Figure 4). In addition, about 13% of NASA mRNAs were relatively
411 enriched in glia cells (Figure S6H), which is consistent with the notion that processes
412 of glia cells contribute to formation of the tripartite synapses[65,66].

413 **Regulation of ac4C and protein levels of memory-related mRNAs by NAT10**

414 Arc, a representative MISA mRNA (Figure 3), is critical for memory[67]. The mRNA of
415 Ca^{2+}/calmodulin-dependent protein kinase 2α (Camk2α) and Grin 2b encode the
416 protein kinase CaMKIIα and the GluN2B subunit of NMDA receptor, respectively.
417 CaMKIIα and GluN2B are synapse-enriched proteins and play important roles in LTP
418 as well as memory[68,69]. Recent studies demonstrate that CaMK2α interaction with
419 GluN2B is critical for the induction and maintenance of LTP[70,71]. Analysis of the low-
420 input acRIP-seq data indicated the reduction of ac4C peaks of Arc, Camk2α and Grin
421 2b mRNAs in the SYN of Nat10 cKO mice, compared with controls (Figures 6E-6G).
422 The genome browser tracks for the ac4C of all NASA mRNAs were accessible at the
423 ac4C website (http://ac4catlas.com/) to show reduced or diminished ac4C peaks in the
424 SYN of Nat10 cKO mice, compared with controls. Despite the presence of a common
425 AGCAGCTG motif in both groups, Nat10 deletion disrupted the local CXX sequence
426 context, reflecting a shift in ac4C deposition specificity upon loss of Nat10 enzymatic
427 activity (Figures S6I). Deconvolution with CIBERSORT identified neurons as the top
428 enriched cell type for both NAT10-dependent and NAT10-independent MISA mRNAs.
429 The neuronal enrichment did not differ between the two sets, which argues against
430 differences in cellular origin (Figure S6J). Moreover, BP enrichment of the 717 shared
431 ac4C-modified mRNAs revealed significant enrichment in biological processes such as
432 synapse organization and dendrite development, indicating a potential role of ac4C
433 modification in regulating synaptic structure and neuronal connectivity (Figure S6K).

434 Next, we performed RT-qPCR analysis for input and acRIP RNAs purified from
435 the SYN of control and Nat10 cKO mice at day 6 after memory to verify the NAT10-

436 dependent ac4C modification of Arc, Camk2α and Grin2b mRNAs. The input mRNA
437 levels of Arc, Camk2α and Grin2b in the SYN were comparable between control and
438 Nat10 cKO mice (Figure 6H). In contrast, the acRIP mRNA levels of Arc, Camk2α and
439 Grin2b in the SYN were significantly reduced in Nat10 cKO mice, compared with
440 controls (Figure 6I). Given that ac4C modification of mRNA has been shown to
441 enhance translation efficiency[19,20], we sought to determine whether NAT10 influences
442 the protein levels of ARC, CaMKIIα and GluN2B in the SYN by western blot analysis.
443 The protein levels of ARC, CaMKIIα and GluN2B were significantly decreased in the
444 SYN at day 6 from Nat10 cKO mice, compared with controls (Figure 6J). Altogether,
445 these results demonstrate that NAT10 regulates ac4C and protein levels of Arc, Camk2α
446 and Grin2b in the SYN of mouse hippocampus at day 6.

447 **Regulation of LTP as well as memory by NAT10 in mouse hippocampus**

448 In the following study, we investigate whether NAT10 in mouse hippocampus is
449 important for synaptic plasticity. The body and brain weight were similar between
450 control and Nat10 cKO mice (Figures S7A and S7B). The number and intrinsic
451 excitability of CA1 pyramidal neurons were also comparable between control and
452 Nat10 cKO mice (Figures S7C and S7D). To address whether NAT10 regulates LTP,
453 we performed electrophysiology recording of fEPSP (field excitatory postsynaptic
454 potential) at the SC-CA1 synapses before and after high frequency stimulation (HFS)
455 (Figure 7A). The induction of LTP was comparable between control and Nat10 cKO
456 mice (Figures 7B-7E). However, the maintenance of LTP especially the late phase of
457 LTP was severely impaired in Nat10 cKO mice, compared with controls (Figures 7B,
458 7C and 7F).

459 To further study whether Nat10 is important for synaptic plasticity after memory,
460 we performed fEPSP recording to investigate glutamatergic transmission at the SC-
461 CA1 synapses in the control and Nat10 cKO mice at day 6 (Figure 7G). Consistent with
462 the previous report[72], the glutamatergic transmission at the SC-CA1 synapses was
463 significantly enhanced at day 6 in memory mice, compared with mice without
464 memory (Figures 7H and 7I). The glutamatergic transmission at the SC-CA1 synapses

465 was similar between control and Nat10 cKO mice without memory, which indicate that
466 Nat10 may be dispensable for the basal glutamatergic transmission at the SC-CA1
467 synapses. However, the memory-induced enhancement of glutamatergic transmission
468 at the SC-CA1 synapses was significantly impaired in Nat10 cKO mice, compared with
469 controls (Figures 7H and 7I). Altogether these results indicate that NAT10 is important
470 for memory-related synaptic plasticity in mouse hippocampus.

471 To investigate whether NAT10 is critical for memory, both control and Nat10 cKO
472 mice were subjected to training in the MWM for 5 days, and the probe test was
473 performed at day 6. Both groups exhibited an overall decline in the latency to reach the
474 platform at the early stage (day 1-2) of training (Figure 7J). However, the Nat10 cKO
475 mice failed to improve performance during the late training stage (day 3-5), compared
476 with controls (Figure 7J). During the probe tests, the control and Nat10 cKO mice
477 showed similar distance travelled (Figures 7K and 7L). However, the time spent in the
478 target area and the number of platform crossing were significantly reduced in the Nat10
479 cKO mice, compared with controls (Figures 7L-7N). These results demonstrate that
480 NAT10 in mouse hippocampus is important for spatial memory.

481

482 **Discussion**

483 In this study, we demonstrated the dynamic regulation of synaptic mRNA acetylation
484 by memory in mouse hippocampus. We identified 1237 MISA mRNAs that were
485 increased in the SYN of mouse hippocampus after memory but returned to normal
486 levels after memories were naturally forgotten. Interestingly, the protein levels of
487 NAT10 were also increased in the SYN after memory but returned to control levels after
488 forgetting. We further showed NAT10-dependent ac4C mapping of SYN mRNAs
489 through the acRIP-seq and verified the NAT10-dependent ac4C modification of Arc,
490 Camk2α and Grin2b mRNAs. The maintenance of LTP at the SC-CA1 synapses as well
491 as the behaviors of memory were severely impaired in the Nat10 cKO mice. In support
492 of the importance of ac4C in memory, our recent study showed that ac4C modification
493 of several MISA mRNAs including Arc, Grin1 and Psen1 was significantly reduced in

494 the hippocampus of 5×FAD mouse, an animal model of Alzheimer's disease that was
495 characterized by deficient synaptic plasticity and memory[73]. Altogether these results
496 demonstrate the importance of NAT10-mediated mRNA acetylation in memory.

497 The dynamic regulation of protein acetylation in the SYN by memory has been
498 shown in our previous studies[74-77]. In contrast to the well-characterized
499 acetyltransferases and deacetylases for protein acetylation[78], the writer and eraser of
500 mRNA acetylation are less well understood. The NAT10 acetyltransferase is the only
501 known ac4C writer in the mammalian cells[24,79]. Recently, the deacetylase SIRT7 has
502 been shown to erase the ac4C modification of ribosomal RNA (rRNA) and small
503 nucleolar RNA (snoRNA)[80,81]. However, the mechanisms underlying the deacetylation
504 of mRNA need further exploration.

505 A pivotal and unexpected finding of our study fundamentally expands the
506 regulatory landscape of ac4C in neurons. We discovered that a substantial fraction of
507 MISA mRNAs (520 out of 1237, approximately 42%) is acetylated in a NAT10-
508 independent manner. This is not a minor detail, but rather points to the existence of a
509 parallel regulatory system for synaptic mRNA acetylation that is co-activated during
510 memory formation. Strikingly, bioinformatic analysis revealed that these NAT10-
511 independent targets possess a consensus motif (RGGGCACTAACY) completely
512 distinct from the canonical motif associated with NAT10. This strongly suggests the
513 involvement of at least one other, as-yet-unidentified, ac4C writer enzyme with a
514 different sequence specificity. This possibility is supported by the reports of NAT10-
515 independent acetylation in other biological contexts[82-84]. The existence of this robust
516 parallel pathway may also explain why the Nat10 cKO phenotype, while significant, is
517 not absolute. This discovery transforms the narrative from a single-enzyme mechanism
518 to a more complex, multi-faceted regulatory network and opens up critical new
519 questions for future research regarding the identity of this novel writer and the
520 functional specialization of these parallel ac4C pathways in synaptic plasticity.

521 How the ac4C modification of mRNA is regulated by neural activities remains
522 largely unknown. Our previous studies showed that overnight starvation downregulated

523 the ac4C modification of tyrosine hydroxylase (TH) mRNA in the sympathetic nerve
524 terminus that innervate the olfactory mucosa in mice, which reduced TH protein levels
525 and dopamine synthesis in the mouse olfactory mucosa after overnight starvation[85]. In
526 this study, we demonstrate that memory regulate the dynamic change of ac4C
527 modification of mRNA at synapses of mouse hippocampus. Altogether these studies
528 provide evidence that neural activities regulate acetylation of mRNA in a
529 spatiotemporally specific manner.

530 NAT10 proteins were increased in the SYN but reduced in the cytoplasm of mouse
531 hippocampus at day 6 in the MWM. These results suggest a relocation of NAT10 from
532 the cytoplasm to synapses after memory, which was corroborated by the
533 immunostaining study of NAT10 distribution in cultured mouse hippocampal neurons
534 after cLTP stimulation. Previous proteomic studies showed that NAT10 were detected
535 in the interactome with several motor proteins such as kinesin proteins[86], which raised
536 the possibility that NAT10 might be transported by the motor proteins in hippocampal
537 neurons during memory. NAT10 was highly expressed in the nucleus of hippocampal
538 neurons, but protein levels of nuclear NAT10 were not altered at day 6 in the MWM.
539 NAT10 has been shown to be important for regulating nuclear functions such as
540 nucleolar assembly[63] and nuclear architecture[87]. The function of NAT10 in the nucleus
541 of neurons waits for future investigations.

542 The subcellular change of NAT10 proteins at day 6 apparently may not be caused
543 by stress during the training in the MWM. The mice were well handled before and
544 during the training, and thus the stress should be minor if any. The control mice were
545 exposed to the training using visible platform at day 1, the stress levels in the control
546 mice may vary with the memory mice. If mild stress during the training in the MWM
547 could cause the relocation of NAT10 to the SYN, the protein levels of NAT10 in the
548 SYN would be increased at day 1. However, the protein levels of NAT10 in the SYN
549 were similar at day 1 between control and memory mice. In addition, chronic mild stress
550 has been shown to increase the total protein levels of NAT10 in mouse hippocampus[88].
551 In contrast, the total protein levels of NAT10 in mouse hippocampus did not alter at day

552 6 in the MWM. These results suggest that the increased NAT10 proteins in the SYN at
553 day 6 in the MWM may be related with memory rather than stress.

554 The stoichiometry levels of ac4C in polyA RNA has been reported to be ~0.2% in
555 HeLa cells[19], ~0.1% in human embryonic stem cells[24], ~0.2% in liver[89], and ~0.3% in
556 heart[25]. Here we showed that ~0.4% of cytidine was acetylated in mouse hippocampus.
557 Although the total protein levels of NAT10 has been reported to be relatively lower in
558 the whole brain tissue compared with reproductive tissues such as testis and ovary[26],
559 the NAT10 was shown to be highly expressed in hippocampal neurons[90]. Future studies
560 are warranted to investigate how the acetyltransferase activity of NAT10 toward mRNA
561 was regulated in different brain regions and different tissues.

562 The basal glutamatergic transmission at the SC-CA1 synapses was unaltered in the
563 Arc knockout mice[91], which is consistent with the phenotypes in the Nat10 cKO mice.
564 On the other hand, ARC has been shown to accelerate AMPA receptor endocytosis[92],
565 and thus the induction of LTP at the SC-CA1 synapses was enhanced in the Arc
566 knockout mice[91]. Although ARC protein levels were decreased in the SYN of Nat10
567 cKO mice, the induction of LTP at the SC-CA1 synapses was not increased in the Nat10
568 cKO mice, which might be due to the reduction of other LTP-promoting proteins such
569 as CaMKIIα and GluN2B in the SYN of Nat10 cKO mice.

570 In line with the phenotypes of Nat10 cKO mice presented in this study, the Arc
571 knockout mice showed deficits in the late phase of LTP at SC-CA1 synapses and
572 impairment of memory consolidation in the MWM[91]. Consistent with the function of
573 Arc in memory consolidation, the acetylation of Arc mRNA was increased in the SYN
574 at day 6 rather than day 1 following MWM training, a period during which memories
575 were consolidated. Furthermore, our findings from cLTP in mouse hippocampal slices
576 suggest that this acetylation process can be induced rapidly. We observed a significant
577 increase in the ac4C levels of Arc mRNA in mouse hippocampal slices one hour after
578 cLTP stimulation, a timescale consistent with the consolidation phase of LTP, for which
579 sustained local synthesis of Arc is known to be critical[67,93]. In sum, the data presented
580 here reveal a novel mechanism underlying how neural activity regulates local protein

synthesis at synapses using Arc as an example.

Although our current study primarily focuses on ac4C modifications of mRNA, we cannot exclude the possibility that Nat10 deficiency also affects post-translational regulatory pathways. Moreover, the function of NAT10 in regulating tRNA or rRNA might also contribute to memory. New techniques for overexpression and erasure of site-specifically acetylated mRNA need to be developed to precisely study the function of mRNA acetylation. Nonetheless, the results presented here provide evidence that NAT10-mediated mRNA acetylation may contribute to the protein synthesis at synapses during memory in mouse hippocampus.

References

1. Shrestha, P., and Klann, E. (2022). Spatiotemporally resolved protein synthesis as a molecular framework for memory consolidation. Trends Neurosci *45*, 297–311. https://doi.org/10.1016/j.tins.2022.01.004.
2. Besse, F., and Ephrussi, A. (2008). Translational control of localized mRNAs: restricting protein synthesis in space and time. Nat Rev Mol Cell Biol *9*, 971–980. https://doi.org/10.1038/nrm2548.
3. Martin, K.C., Barad, M., and Kandel, E.R. (2000). Local protein synthesis and its role in synapse-specific plasticity. Curr Opin Neurobiol *10*, 587–592. https://doi.org/10.1016/s0959-4388(00)00128-8.
4. Sutton, M.A., and Schuman, E.M. (2006). Dendritic protein synthesis, synaptic plasticity, and memory. Cell *127*, 49–58. https://doi.org/10.1016/j.cell.2006.09.014.
5. Day, J.J., and Sweatt, J.D. (2011). Epigenetic mechanisms in cognition. Neuron *70*, 813–829. https://doi.org/10.1016/j.neuron.2011.05.019.
6. Levenson, J.M., and Sweatt, J.D. (2005). Epigenetic mechanisms in memory formation. Nat Rev Neurosci *6*, 108–118. https://doi.org/10.1038/nrn1604.
7. Fischer, A., Sananbenesi, F., Wang, X., Dobbin, M., and Tsai, L.-H. (2007). Recovery of learning and memory is associated with chromatin remodelling. Nature *447*, 178–182. https://doi.org/10.1038/nature05772.
8. Levenson, J.M., O'Riordan, K.J., Brown, K.D., Trinh, M.A., Molfese, D.L., and Sweatt, J.D. (2004). Regulation of histone acetylation during memory formation in the hippocampus. J Biol Chem *279*, 40545–40559. https://doi.org/10.1074/jbc.M402229200.
9. Kouzarides, T. (2007). Chromatin modifications and their function. Cell *128*, 693–705. https://doi.org/10.1016/j.cell.2007.02.005.
10. Merkurjev, D., Hong, W.-T., Iida, K., Oomoto, I., Goldie, B.J., Yamaguti, H., Ohara, T., Kawaguchi, S.-y., Hirano, T., and Martin, K.C. (2018). Synaptic N 6-methyladenosine (m6A) epitranscriptome reveals functional partitioning of

localized transcripts. Nat Neurosci *21*, 1004–1014. https://doi.org/10.1038/s41593-018-0173-6.

11. Zhuang, M., Geng, X., Han, P., Che, P., Liang, F., Liu, C., Yang, L., Yu, J., Zhang, Z., Dong, W., and Ji, S.-J. (2023). YTHDF2 in dentate gyrus is the m6A reader mediating m6A modification in hippocampus-dependent learning and memory. Mol Psychiatry *28*, 1679–1691. https://doi.org/10.1038/s41380-023-01953-z.
12. Shi, H., Zhang, X., Weng, Y.-L., Lu, Z., Liu, Y., Lu, Z., Li, J., Hao, P., Zhang, Y., Zhang, F., et al. (2018). m6A facilitates hippocampus-dependent learning and memory through YTHDF1. Nature *563*, 249–253. https://doi.org/10.1038/s41586-018-0666-1.
13. Boccaletto, P., Machnicka, M.A., Purta, E., Piątkowski, P., Bagiński, B., Wirecki, T.K., de Crécy-Lagard, V., Ross, R., Limbach, P.A., and Kotter, A. (2018). MODOMICS: a database of RNA modification pathways. 2017 update. Nucleic Acids Res *46*, D303–D307. https://doi.org/10.1093/nar/gkx1030.
14. Stern, L., and LH, S. (1978). The role of the minor base N4-acetylcytidine in the function of the Escherichia coli noninitiator methionine transfer RNA. J Biol Chem *17*, 6132–6139. https://doi.org/10.1016/s0021-9258(17)34590-8.
15. Oashi, Z., Murao, K., Yahagi, T., Von Minden, D.L., McCloskey, J.A., and Nishimura, S. (1972). Characterization of C + located in the first position of the anticodon of Escherichia coli tRNA Met as N 4 -acetylcytidine. Biochim Biophys Acta *262*, 209–213. https://doi.org/10.1016/0005-2787(72)90234-1.
16. Kowalski, S., Yamane, T., and Fresco, J.R. (1971). Nucleotide sequence of the "denaturable" leucine transfer RNA from yeast. Science *172*, 385–387. https://doi.org/10.1126/science.172.3981.385.
17. Kruppa, J., and Zachau, H.G. (1972). Multiplicity of serine-specific transfer RNAs of brewer's and baker's yeast. Biochim Biophys Acta *277*, 499–512. https://doi.org/10.1016/0005-2787(72)90093-7.
18. Ito, S., Akamatsu, Y., Noma, A., Kimura, S., Miyauchi, K., Ikeuchi, Y., Suzuki, T., and Suzuki, T. (2014). A single acetylation of 18 S rRNA is essential for biogenesis of the small ribosomal subunit in Saccharomyces cerevisiae. J Biol Chem *289*, 26201–26212. https://doi.org/10.1074/jbc.M114.593996.
19. Arango, D., Sturgill, D., Alhusaini, N., Dillman, A.A., Sweet, T.J., Hanson, G., Hosogane, M., Sinclair, W.R., Nanan, K.K., and Mandler, M.D. (2018). Acetylation of cytidine in mRNA promotes translation efficiency. Cell *175*, 1872–1886. e1824. https://doi.org/10.1016/j.cell.2018.10.030
20. Arango, D., Sturgill, D., Yang, R., Kanai, T., Bauer, P., Roy, J., Wang, Z., Hosogane, M., Schiffers, S., and Oberdoerffer, S. (2022). Direct epitranscriptomic regulation of mammalian translation initiation through N4-acetylcytidine. Mol Cell *82*, 2797–2814. e2711. https://doi.org/10.1016/j.molcel.2022.05.016.
21. Ito, S., Horikawa, S., Suzuki, T., Kawauchi, H., Tanaka, Y., Suzuki, T., and Suzuki, T. (2014). Human NAT10 is an ATP-dependent RNA acetyltransferase responsible for N4-acetylcytidine formation in 18 S ribosomal RNA (rRNA). J Biol Chem *289*, 35724–35730. https://doi.org/10.1074/jbc.C114.602698.

22. Liu, Y., Wang, X., Liu, Y., Yang, J., Mao, W., Feng, C., Wu, X., Chen, X., Chen, L., and Dong, P. (2023). N4-acetylcytidine-dependent GLMP mRNA stabilization by NAT10 promotes head and neck squamous cell carcinoma metastasis and remodels tumor microenvironment through MAPK/ERK signaling pathway. Cell Death Dis *14*, 712. https://doi.org/10.1038/s41419-023-06245-6.
23. Wang, G., Zhang, M., Zhang, Y., Xie, Y., Zou, J., Zhong, J., Zheng, Z., Zhou, X., Zheng, Y., and Chen, B. (2022). NAT10-mediated mRNA N4-acetylcytidine modification promotes bladder cancer progression. Clin Transl Med *12*, e738. https://doi.org/10.1002/ctm2.738.
24. Hu, Z., Lu, Y., Cao, J., Lin, L., Chen, X., Zhou, Z., Pu, J., Chen, G., Ma, X., and Deng, Q. (2024). N-acetyltransferase NAT10 controls cell fates via connecting mRNA cytidine acetylation to chromatin signaling. Sci Adv *10*, eadh9871. https://doi.org/10.1126/sciadv.adh9871.
25. Shi, J., Yang, C., Zhang, J., Zhao, K., Li, P., Kong, C., Wu, X., Sun, H., Zheng, R., and Sun, W. (2023). NAT10 is involved in cardiac remodeling through ac4C-mediated transcriptomic regulation. Circ Res *133*, 989–1002. https://doi.org/10.1161/CIRCRESAHA.122.322244.
26. Jiang, X., Cheng, Y., Zhu, Y., Xu, C., Li, Q., Xing, X., Li, W., Zou, J., Meng, L., and Azhar, M. (2023). Maternal NAT10 orchestrates oocyte meiotic cell-cycle progression and maturation in mice. Nat Commun *14*, 3729. https://doi.org/10.1038/s41467-023-39256-0.
27. Zhang, M., Yang, K., Wang, Q.-H., Xie, L., Liu, Q., Wei, R., Tao, Y., Zheng, H.-L., Lin, N., and Xu, H. (2023). The cytidine N-acetyltransferase NAT10 participates in peripheral nerve injury-induced neuropathic pain by stabilizing SYT9 expression in primary sensory neurons. J Neurosci *43*, 3009–3027. https://doi.org/10.1523/JNEUROSCI.2321-22.2023.
28. Xu, T., Wang, J., Wu, Y., Wu, J.Y., Lu, W.C., Liu, M., Zhang, S.B., Xie, D., Xin, W.J., and Xie, J.D. (2023). Ac4C Enhances the Translation Efficiency of Vegfa mRNA and Mediates Central Sensitization in Spinal Dorsal Horn in Neuropathic Pain. Adv Sci *10*, e2303113. https://doi.org/10.1002/advs.202303113.
29. Jarrard, L.E. (1993). On the role of the hippocampus in learning and memory in the rat. Behav Neural Biol *60*, 9–26. https://doi.org/10.1016/0163-1047(93)90664-4.
30. Moser, M.-B., Trommald, M., and Andersen, P. (1994). An increase in dendritic spine density on hippocampal CA1 pyramidal cells following spatial learning in adult rats suggests the formation of new synapses. Proc Natl Acad Sci U S A *91*, 12673–12675. https://doi.org/10.1073/pnas.91.26.12673.
31. Morris, R. (1984). Developments of a water-maze procedure for studying spatial learning in the rat. J Neurosci Methods *11*, 47–60. https://doi.org/10.1016/0165-0270(84)90007-4.
32. Bliss, T.V., and Collingridge, G.L. (1993). A synaptic model of memory: long-term potentiation in the hippocampus. Nature *361*, 31–39.

https://doi.org/10.1038/361031a0.
33. Biever, A., Glock, C., Tushev, G., Ciirdaeva, E., Dalmay, T., Langer, J.D., and Schuman, E.M. (2020). Monosomes actively translate synaptic mRNAs in neuronal processes. Science *367*, eaay4991. https://doi.org/10.1126/science.aay4991.
34. Goldie, B.J., and Cairns, M.J. (2012). Post-transcriptional trafficking and regulation of neuronal gene expression. Mol Neurobiol *45*, 99–108. https://doi.org/10.1007/s12035-011-8222-0.
35. Beiki, H., Sturgill, D., Arango, D., Relier, S., Schiffers, S., and Oberdoerffer, S. (2024). Detection of ac4C in human mRNA is preserved upon data reassessment. Mol Cell *84*, 1611–1625. e1613. https://doi.org/10.1016/j.molcel.2024.03.018.
36. Georgeson, J., and Schwartz, S. (2024). No evidence for ac4C within human mRNA upon data reassessment. Mol Cell *84*, 1601–1610. e1602. https://doi.org/10.1016/j.molcel.2024.03.017.
37. Li, B., Xi, W., Bai, Y., Liu, X., Zhang, Y., Li, L., Bian, L., Liu, C., Tang, Y., Shen, L., et al. (2023). FTO-dependent m(6)A modification of Plpp3 in circSCMH1-regulated vascular repair and functional recovery following stroke. Nat Commun *14*, 489. https://doi.org/10.1038/s41467-023-36008-y.
38. Sinclair, W.R., Arango, D., Shrimp, J.H., Zengeya, T.T., Thomas, J.M., Montgomery, D.C., Fox, S.D., Andresson, T., Oberdoerffer, S., and Meier, J.L. (2017). Profiling cytidine acetylation with specific affinity and reactivity. ACS Chem Biol *12*, 2922–2926. https://doi.org/10.1021/acschembio.7b00734.
39. Yu, F., Zhang, Y., Cheng, C., Wang, W., Zhou, Z., Rang, W., Yu, H., Wei, Y., Wu, Q., and Zhang, Y. (2020). Poly (A)-seq: A method for direct sequencing and analysis of the transcriptomic poly (A)-tails. PloS one *15*, e0234696. https://doi.org/10.1371/journal.pone.0234696.
40. Vorhees, C.V., and Williams, M.T. (2006). Morris water maze: procedures for assessing spatial and related forms of learning and memory. Nat Protoc *1*, 848–858. https://doi.org/10.1038/nprot.2006.116.
41. Hoz, L.d., Martin, S.J., and Morris, R.G.M. (2004). Forgetting, reminding, and remembering: the retrieval of lost spatial memory. PLoS Biol *2*, e225. https://doi.org/10.1371/journal.pbio.0020225.
42. Zhang, W., Gao, J., Fan, L., Wang, J., He, B., Wang, Y., Zhang, X., and Mao, H. (2023). ac4C acetylation regulates mRNA stability and translation efficiency in osteosarcoma. Heliyon *9*, e17103. https://doi.org/10.1016/j.heliyon.2023.e17103.
43. Cajigas, I.J., Tushev, G., Will, T.J., tom Dieck, S., Fuerst, N., and Schuman, E.M. (2012). The local transcriptome in the synaptic neuropil revealed by deep sequencing and high-resolution imaging. Neuron *74*, 453–466. https://doi.org/10.1016/j.neuron.2012.02.036.
44. Hafner, A.S., Donlin Asp, P.G., Leitch, B., Herzog, E., and Schuman, E.M. (2019). Local protein synthesis is a ubiquitous feature of neuronal pre-and postsynaptic compartments. Science *364*, eaau3644. https://doi.org/10.1126/science.aau3644.

45. Niu, M., Cao, W., Wang, Y., Zhu, Q., Luo, J., Wang, B., Zheng, H., Weitz, D.A., and Zong, C. (2023). Droplet-based transcriptome profiling of individual synapses. Nat Biotechnol *41*, 1332–1344. https://doi.org/10.1038/s41587-022-01635-1.
46. Steward, O., Wallace, C.S., Lyford, G.L., and Worley, P.F. (1998). Synaptic activation causes the mRNA for the IEG Arc to localize selectively near activated postsynaptic sites on dendrites. Neuron *21*, 741–751. https://doi.org/10.1016/s0896-6273(00)80591-7.
47. Lyford, G.L., Yamagata, K., Kaufmann, W.E., Barnes, C.A., Sanders, L.K., Copeland, N.G., Gilbert, D.J., Jenkins, N.A., Lanahan, A.A., and Worley, P.F. (1995). Arc, a growth factor and activity-regulated gene, encodes a novel cytoskeleton-associated protein that is enriched in neuronal dendrites. Neuron *14*, 433–445. https://doi.org/10.1016/0896-6273(95)90299-6.
48. Das, S., Lituma, P.J., Castillo, P.E., and Singer, R.H. (2023). Maintenance of a short-lived protein required for long-term memory involves cycles of transcription and local translation. Neuron *111*, 2051–2064 e2056. https://doi.org/10.1016/j.neuron.2023.04.005.
49. Steward, O., Farris, S., Pirbhoy, P.S., Darnell, J., and Driesche, S.J. (2015). Localization and local translation of Arc/Arg3.1 mRNA at synapses: some observations and paradoxes. Front Mol Neurosci *7*, 101. https://doi.org/10.3389/fnmol.2014.00101.
50. Bramham, C.R., Alme, M.N., Bittins, M., Kuipers, S.D., Nair, R.R., Pai, B., Panja, D., Schubert, M., Soule, J., Tiron, A., and Wibrand, K. (2010). The Arc of synaptic memory. Exp Brain Res *200*, 125–140. https://doi.org/10.1007/s00221-009-1959-2.
51. Yu, Q., Liu, Y.-Z., Zhu, Y.-B., Wang, Y.-Y., Li, Q., and Yin, D.-M. (2019). Genetic labeling reveals temporal and spatial expression pattern of D2 dopamine receptor in rat forebrain. Brain Struct Funct *224*, 1035–1049. https://doi.org/10.1007/s00429-018-01824-2.
52. Madisen, L., Zwingman, T.A., Sunkin, S.M., Oh, S.W., Zariwala, H.A., Gu, H., Ng, L.L., Palmiter, R.D., Hawrylycz, M.J., and Jones, A.R. (2010). A robust and high-throughput Cre reporting and characterization system for the whole mouse brain. Nat Neurosci *13*, 133–140. https://doi.org/10.1038/nn.2467.
53. Biane, J.S., Ladow, M.A., Stefanini, F., Boddu, S.P., Fan, A., Hassan, S., Dundar, N., Apodaca-Montano, D.L., Zhou, L.Z., and Fayner, V. (2023). Neural dynamics underlying associative learning in the dorsal and ventral hippocampus. Nat Neurosci *26*, 798–809. https://doi.org/10.1038/s41593-023-01296-6.
54. Fanselow, M.S., and Dong, H.-W. (2010). Are the dorsal and ventral hippocampus functionally distinct structures? Neuron *65*, 7–19. https://doi.org/10.1016/j.neuron.2009.11.031.
55. Moser, E., Moser, M.-B., and Andersen, P. (1993). Spatial learning impairment parallels the magnitude of dorsal hippocampal lesions, but is hardly present following ventral lesions. J Neurosci *13*, 3916–3925. https://doi.org/10.1523/JNEUROSCI.13-09-03916.1993.

56. Lau, O.D., Courtney, A.D., Vassilev, A., Marzilli, L.A., Cotter, R.J., Nakatani, Y., and Cole, P.A. (2000). p300/CBP-associated factor histone acetyltransferase processing of a peptide substrate: kinetic analysis of the catalytic mechanism. J Biol Chem *275*, 21953–21959. https://doi.org/10.1074/jbc.M003219200.
57. Shahi, K., and Baudry, M. (1993). Glycine-induced changes in synaptic efficacy in hippocampal slices involve changes in AMPA receptors. Brain Res *627*, 261–266. https://doi.org/10.1016/0006-8993(93)90329-l.
58. Lu, W., Man, H., Ju, W., Trimble, W.S., MacDonald, J.F., and Wang, Y.T. (2001). Activation of synaptic NMDA receptors induces membrane insertion of new AMPA receptors and LTP in cultured hippocampal neurons. Neuron *29*, 243–254. https://doi.org/10.1016/s0896-6273(01)00194-5.
59. Yin, Y., Edelman, G.M., and Vanderklish, P.W. (2002). The brain-derived neurotrophic factor enhances synthesis of Arc in synaptoneurosomes. Proceedings of the National Academy of Sciences *99*, 2368–2373. https://doi.org/10.1073/pnas.042693699.
60. Tsien, J.Z., Chen, D.F., Gerber, D., Tom, C., Mercer, E.H., Anderson, D.J., Mayford, M., Kandel, E.R., and Tonegawa, S. (1996). Subregion-and cell type–restricted gene knockout in mouse brain. Cell *87*, 1317–1326. https://doi.org/10.1016/s0092-8674(00)81826-7.
61. Hedegaard, C., Kjaer-Sorensen, K., Madsen, L.B., Henriksen, C., Momeni, J., Bendixen, C., Oxvig, C., and Larsen, K. (2013). Porcine synapsin 1: SYN1 gene analysis and functional characterization of the promoter. FEBS Open Bio *3*, 411–420. https://doi.org/10.1016/j.fob.2013.10.002.
62. Lv, J., Liu, H., Wang, Q., Tang, Z., Hou, L., and Zhang, B. (2003). Molecular cloning of a novel human gene encoding histone acetyltransferase-like protein involved in transcriptional activation of hTERT. Biochem Biophys Res Commun *311*, 506–513. https://doi.org/10.1016/j.bbrc.2003.09.235.
63. Shen, Q., Zheng, X., McNutt, M.A., Guang, L., Sun, Y., Wang, J., Gong, Y., Hou, L., and Zhang, B. (2009). NAT10, a nucleolar protein, localizes to the midbody and regulates cytokinesis and acetylation of microtubules. Exp Cell Res *315*, 1653–1667. https://doi.org/10.1016/j.yexcr.2009.03.007.
64. Saunders, A., Macosko, E.Z., Wysoker, A., Goldman, M., Krienen, F.M., de Rivera, H., Bien, E., Baum, M., Bortolin, L., Wang, S., et al. (2018). Molecular Diversity and Specializations among the Cells of the Adult Mouse Brain. Cell *174*, 1015–1030 e1016. https://doi.org/10.1016/j.cell.2018.07.028.
65. Perea, G., Navarrete, M., and Araque, A. (2009). Tripartite synapses: astrocytes process and control synaptic information. Trends Neurosci *32*, 421–431. https://doi.org/10.1016/j.tins.2009.05.001.
66. Eroglu, C., and Barres, B.A. (2010). Regulation of synaptic connectivity by glia. Nature *468*, 223–231. https://doi.org/10.1038/nature09612.
67. Bramham, C.R., Worley, P.F., Moore, M.J., and Guzowski, J.F. (2008). The immediate early gene arc/arg3. 1: regulation, mechanisms, and function. Journal of Neuroscience *28*, 11760–11767. https://doi.org/10.1523/JNEUROSCI.3864-08.2008.

68. Lisman, J., Yasuda, R., and Raghavachari, S. (2012). Mechanisms of CaMKII action in long-term potentiation. Nat Rev Neurosci *13*, 169–182. https://doi.org/10.1038/nrn3192.
69. Tang, Y.P., Shimizu, E., Dube, G.R., Rampon, C., Kerchner, G.A., Zhuo, M., Liu, G., and Tsien, J.Z. (1999). Genetic enhancement of learning and memory in mice. Nature *401*, 63–69. https://doi.org/10.1038/43432.
70. Tullis, J.E., Larsen, M.E., Rumian, N.L., Freund, R.K., Boxer, E.E., Brown, C.N., Coultrap, S.J., Schulman, H., Aoto, J., Dell'Acqua, M.L., and Bayer, K.U. (2023). LTP induction by structural rather than enzymatic functions of CaMKII. Nature *621*, 146–153. https://doi.org/10.1038/s41586-023-06465-y.
71. Chen, X., Cai, Q., Zhou, J., Pleasure, S.J., Schulman, H., Zhang, M., and Nicoll, R.A. (2024). CaMKII autophosphorylation is the only enzymatic event required for synaptic memory. Proc Natl Acad Sci U S A *121*, e2402783121. https://doi.org/10.1073/pnas.240278312.
72. Su, J., Huang, F., Tian, Y., Tian, R., Qianqian, G., Bello, S.T., Zeng, D., Jendrichovsky, P., Lau, C.G., and Xiong, W. (2023). Entorhinohippocampal cholecystokinin modulates spatial learning by facilitating neuroplasticity of hippocampal CA3-CA1 synapses. Cell Rep *42*, 113467. https://doi.org/10.1016/j.celrep.2023.113467.
73. Ji, H.-N., Zhou, H.-Q., Qie, J.-B., Lu, W.-M., Gao, H.-T., and Wu, D.-H. (2025). Dysregulated ac4C modification of mRNA in a mouse model of early-stage Alzheimer's disease. Cell & Bioscience *15*, 45. https://doi.org/10.1186/s13578-025-01389-8.
74. Zhang, H.-L., Han, W., Du, Y.-Q., Zhao, B., Yang, P., and Yin, D.-M. (2021). SRC3 acetylates calmodulin in the mouse brain to regulate synaptic plasticity and fear learning. J Biol Chem *297*, 101044. https://doi.org/10.1016/j.jbc.2021.101044.
75. Zhang, H.-L., Zhao, B., Han, W., Sun, Y.-B., Yang, P., Chen, Y., Ni, D., Zhang, J., and Yin, D.-M. (2021). Acetylation of calmodulin regulates synaptic plasticity and fear learning. J Biol Chem *297*, 101034. https://doi.org/10.1016/j.jbc.2021.101034.
76. Zhang, H.-L., Zhao, B., Yang, P., Du, Y.-Q., Han, W., Xu, J., and Yin, D.-M. (2021). Steroid receptor coactivator 3 regulates synaptic plasticity and hippocampus-dependent memory. Neurosci Bull *37*, 1645–1657. https://doi.org/10.1007/s12264-021-00741-5.
77. Zhang, H.L., Hu, S., Yang, P., Long, H.C., Ma, Q.H., Yin, D.M., and Xu, G.Y. (2024). HDAC9-mediated calmodulin deacetylation induces memory impairment in Alzheimer's disease. CNS Neurosci Ther *30*, e14573. https://doi.org/10.1111/cns.14573.
78. Drazic, A., Myklebust, L.M., Ree, R., and Arnesen, T. (2016). The world of protein acetylation. Biochim Biophys Acta *1864*, 1372–1401. https://doi.org/10.1016/j.bbapap.2016.06.007.
79. Cui, Z., Xu, Y., Wu, P., Lu, Y., Tao, Y., Zhou, C., Cui, R., Li, J., and Han, R. (2023). NAT10 promotes osteogenic differentiation of periodontal ligament

stem cells by regulating VEGFA-mediated PI3K/AKT signaling pathway through ac4C modification. Odontology *111*, 870–882. https://doi.org/10.1007/s10266-023-00793-1.

80. Xu, C., Zhang, J., Zhang, J., and Liu, B. (2021). SIRT7 is a deacetylase of N4-acetylcytidine on ribosomal RNA. Genome Instab Dis *2*, 253–260. https://doi.org/10.1007/s42764-021-00046-x.

81. Kudrin, P., Meierhofer, D., Vågbø, C.B., and Ørom, U.A.V. (2021). Nuclear RNA-acetylation can be erased by the deacetylase SIRT7. BioRxiv, 2021.2004.2006.438707. https://doi.org/10.1101/2021.04.06.438707.

82. Svobodová Kovaříková, A., Stixová, L., Kovařík, A., and Bártová, E. (2023). PARP-dependent and NAT10-independent acetylation of N4-cytidine in RNA appears in UV-damaged chromatin. Epigenetics & Chromatin *16*, 26. https://doi.org/10.1186/s13072-023-00501-x.

83. Schiffers, S., and Oberdoerffer, S. (2024). ac4C: a fragile modification with stabilizing functions in RNA metabolism. RNA *30*, 583–594. https://doi.org/10.1261/rna.079948.124.

84. Liu, R., Wubulikasimu, Z., Cai, R., Meng, F., Cui, Q., Zhou, Y., and Li, Y. (2023). NAT10-mediated N4-acetylcytidine mRNA modification regulates self-renewal in human embryonic stem cells. Nucleic acids research *51*, 8514–8531. https://doi.org/10.1093/nar/gkad628.

85. Zhou, H.-Q., Zhuang, L.-J., Bao, H.-Q., Li, S.-J., Dai, F.-Y., Wang, P., Li, Q., and Yin, D.-M. (2022). Olfactory regulation by dopamine and DRD2 receptor in the nose. Proc Natl Acad Sci U S A *119*, e2118570119. https://doi.org/10.1073/pnas.2118570119.

86. Rouillard, A.D., Gundersen, G.W., Fernandez, N.F., Wang, Z., Monteiro, C.D., McDermott, M.G., and Ma'ayan, A. (2016). The harmonizome: a collection of processed datasets gathered to serve and mine knowledge about genes and proteins. Database (Oxford) *2016*, 2016:baw2100. https://doi.org/10.1093/database/baw100.

87. Larrieu, D., Britton, S., Demir, M., Rodriguez, R., and Jackson, S.P. (2014). Chemical inhibition of NAT10 corrects defects of laminopathic cells. Science *344*, 527–532. https://doi.org/10.1126/science.1252651.

88. Guo, X.-F., Wang, X.-H., Fu, Y.-L., Meng, Q., Huang, B.-Y., Yang, R., Guo, Y., Du, Y.-R., Wang, X., and Gao, Y. (2022). Elevation of N-acetyltransferase 10 in hippocampal neurons mediates depression-and anxiety-like behaviors. Brain Res Bull *185*, 91–98. https://doi.org/10.1016/j.brainresbull.2022.05.004.

89. Hao, H., Liu, W., Miao, Y., Ma, L., Yu, B., Liu, L., Yang, C., Zhang, K., Chen, Z., Yang, J., et al. (2022). N4-acetylcytidine regulates the replication and pathogenicity of enterovirus 71. Nucleic Acids Res *50*, 9339–9354. https://doi.org/10.1093/nar/gkac675.

90. Gao, S., Shen, R., Li, J., Jiang, Y., Sun, H., Wu, X., Li, X., Miao, C., He, M., Wang, J., and Chen, W. (2024). N-acetyltransferase 10 mediates cognitive dysfunction through the acetylation of GABABR1 mRNA in sepsis-associated encephalopathy. Proc Natl Acad Sci U S A *121*, e2410564121.

https://doi.org/10.1073/pnas.2410564121.

91. Plath, N., Ohana, O., Dammermann, B., Errington, M.L., Schmitz, D., Gross, C., Mao, X., Engelsberg, A., Mahlke, C., and Welzl, H. (2006). Arc/Arg3. 1 is essential for the consolidation of synaptic plasticity and memories. Neuron *52*, 437–444. https://doi.org/10.1016/j.neuron.2006.08.024.

92. Chowdhury, S., Shepherd, J.D., Okuno, H., Lyford, G., Petralia, R.S., Plath, N., Kuhl, D., Huganir, R.L., and Worley, P.F. (2006). Arc/Arg3.1 interacts with the endocytic machinery to regulate AMPA receptor trafficking. Neuron *52*, 445–459. https://doi.org/10.1016/j.neuron.2006.08.033.

93. Messaoudi, E., Kanhema, T., Soulé, J., Tiron, A., Dagyte, G., da Silva, B., and Bramham, C.R. (2007). Sustained Arc/Arg3.1 synthesis controls long-term potentiation consolidation through regulation of local actin polymerization in the dentate gyrus in vivo. Journal of Neuroscience *27*, 10445–10455. https://doi.org/10.1523/JNEUROSCI.2883-07.2007.

94. Guzowski, J.F., Setlow, B., Wagner, E.K., and McGaugh, J.L. (2001). Experience-dependent gene expression in the rat hippocampus after spatial learning: a comparison of the immediate-early genesArc, c-fos, and zif268. Journal of Neuroscience *21*, 5089–5098. https://doi.org/10.1523/JNEUROSCI.21-14-05089.2001.

95. Ting, A.K., Chen, Y., Wen, L., Yin, D.M., Shen, C., Tao, Y., Liu, X., Xiong, W.C., and Mei, L. (2011). Neuregulin 1 promotes excitatory synapse development and function in GABAergic interneurons. J Neurosci *31*, 15–25. https://doi.org/10.1523/jneurosci.2538-10.2011.

96. Wu, D., Bacaj, T., Morishita, W., Goswami, D., Arendt, K.L., Xu, W., Chen, L., Malenka, R.C., and Südhof, T.C. (2017). Postsynaptic synaptotagmins mediate AMPA receptor exocytosis during LTP. Nature *544*, 316–321. https://doi.org/10.1038/nature21720.

97. Thalalla Gamage, S., Sas-Chen, A., Schwartz, S., and Meier, J.L. (2021). Quantitative nucleotide resolution profiling of RNA cytidine acetylation by ac4C-seq. Nat Protoc *16*, 2286–2307. https://doi.org/10.1038/s41596-021-00501-9.

98. Zhang, Y., Liu, T., Meyer, C.A., Eeckhoute, J., Johnson, D.S., Bernstein, B.E., Nusbaum, C., Myers, R.M., Brown, M., Li, W., and Liu, X.S. (2008). Model-based Analysis of ChIP-Seq (MACS). Genome Biol *9*, R137. https://doi.org/10.1186/gb-2008-9-9-r137.

99. Heinz, S., Benner, C., Spann, N., Bertolino, E., Lin, Y.C., Laslo, P., Cheng, J.X., Murre, C., Singh, H., and Glass, C.K. (2010). Simple combinations of lineage-determining transcription factors prime cis-regulatory elements required for macrophage and B cell identities. Mol Cell *38*, 576–589. https://doi.org/10.1016/j.molcel.2010.05.004.

100. Wu, T., Hu, E., Xu, S., Chen, M., Guo, P., Dai, Z., Feng, T., Zhou, L., Tang, W., and Zhan, L. (2021). clusterProfiler 4.0: A universal enrichment tool for interpreting omics data. Innovation (Camb) *2*, 100141. https://doi.org/10.1016/j.xinn.2021.100141.

101. Guca, E., Alarcon, R., Palo, M.Z., Santos, L., Alonso-Gil, S., Davyt, M., de Lima, L.H., Boissier, F., Das, S., and Zagrovic, B. (2024). N6-methyladenosine in 5′ UTR does not promote translation initiation. Mol Cell *84*, 584–595. e586. https://doi.org/10.1016/j.molcel.2023.12.028
102. Newman, A.M., Liu, C.L., Green, M.R., Gentles, A.J., Feng, W., Xu, Y., Hoang, C.D., Diehn, M., and Alizadeh, A.A. (2015). Robust enumeration of cell subsets from tissue expression profiles. Nat Methods *12*, 453–457. https://doi.org/10.1038/nmeth.3337.
103. Tan, G.H., Liu, Y.Y., Hu, X.L., Yin, D.M., Mei, L., and Xiong, Z.Q. (2011). Neuregulin 1 represses limbic epileptogenesis through ErbB4 in parvalbumin-expressing interneurons. Nat Neurosci *15*, 258–266. https://doi.org/10.1038/nn.3005.
104. Yin, D.-M., Chen, Y.-J., Lu, Y.-S., Bean, J.C., Sathyamurthy, A., Shen, C., Liu, X., Lin, T.W., Smith, C.A., and Xiong, W.-C. (2013). Reversal of behavioral deficits and synaptic dysfunction in mice overexpressing neuregulin 1. Neuron *78*, 644–657. https://doi.org/10.1016/j.neuron.2013.03.028.

Methods

Animals

Male C57BL/6 mice were used throughout this study. For stereotaxic injection of AAV, six-week-old mice were used. For behavioral analysis, 9 to 10-week-old mice were used. For ac4C dot-blots, LC-MS/MS, acRIP-seq, mice aged between nine and ten weeks were used. For immunofluorescence, western blots and electrophysiology, ten-week-old mice were used. Animals were housed in rooms at 23°C and 50% humidity in a 12 h light/dark cycle and with food and water available ad libitum. Animal experimental procedures were approved by the Institutional Animal Care and Use Committee of East China Normal University. The Ai14 Cre-dependent tdTomato reporter mouse line (stock no. 007914) was obtained and used for generating reporter mice.

Generation of Nat10$^{Cre/+}$ knockin mice

The mouse Nat10 gene has 29 exons and the translational start codon (ATG) is localized in exon 2. We employed CRISPR/Cas9 technology in conjunction with homologous recombination to insert a Cre-WPRE-polyA expression cassette at the translational start codon of the Nat10 gene in C57BL/6J mice. The process commenced with the synthesis of Cas9 mRNA and a guide RNA (gRNA) targeting the start codon of Nat10, with the gRNA sequence being 5′-catcatgaatcggaagaaggtgg-3′. A donor vector was then constructed using In-Fusion cloning, containing 2.6 kb 5′ and 3′ homology arms flanking the Cre-WPRE-pA cassette, designed for Cre recombinase expression, enhanced by the WPRE element and concluded with a polyadenylation signal. The

cocktail of Cas9 mRNA, gRNA, and the donor vector was microinjected into fertilized C57BL/6J mouse embryos, leading to the birth of F0 generation mice. These mice were screened for the precise genomic integration of the cassette through PCR amplification and sequencing. Successful modifications were observed in F0 mice, which were subsequently bred with C57BL/6J mice to secure F1 progeny harboring the modification.

The resulting offspring were genotyped using PCR, with primers designed to detect the Cre within the Nat10 gene. The primers for genotyping wt Nat10 allele are as follows: forward: 5’tgtctttcctgtggtggtgt3’; reverse: 5’tgcgcactgaaaccctacaa3’. the primers for genotyping Nat10-cre allele are as follows: forward: 5’gaaatcatgcaggctggtgg3’; reverse: 5’aaagtcccggaaaggagctg3’. The PCR products for wt Nat10 and Nat10-Cre alleles were 392 and 393 bp, respectively.

Generation of Nat10$^{flox/flox}$ mice

The generation of Nat10$^{flox/flox}$ mice involved targeted modification of exon 4 within the Nat10 gene, utilizing CRISPR/Cas9-mediated gene editing. Two guide RNAs (gRNAs) were specifically designed to target and flank exon 4, enabling a precise floxed modification. The sequences for these gRNAs were as follows: gRNA1: 5′-tcagcagaccactttaaagatgg-3′ and gRNA2: 5′-tgcctgacatagtaaggtctggg-3′. Both Cas9 mRNA and gRNAs were produced through in vitro transcription techniques. A donor vector for homologous recombination was constructed using In-Fusion cloning. This vector included a 3.0 kb 5′ homology arm, a 0.7 kb loxp-flanked region (flox), and a 3.0 kb 3′ homology arm to ensure accurate genomic insertion at the Nat10 locus. The mixture of Cas9 mRNA and the two gRNAs was injected into the cytoplasm of one-cell stage embryos. These embryos were subsequently implanted into pseudopregnant females and carried to term. The resulting offspring were genotyped using PCR, with primers designed to detect the floxed exon 4 of Nat10 gene. The primers for genotyping the wt and floxed Nat10 allele are as follows: forward: 5’tgccgaggggatgtactcat3’; reverse: 5’agaaccccacgaactgtcct3’. The PCR products for wt Nat10 and floxed Nat10 allele were 302 and 356 bp, respectively.

Morris water maze (MWM)

The MWM, a widely recognized method for assessing spatial memory[40], was implemented with the following protocol: mice were acclimated to the testing environment over a period of three days through 10-minute daily handling sessions. To

aid navigation, visual cues were strategically positioned around the perimeter of the maze. To ensure consistency and minimize the impact of external variables, all experimental sessions were conducted simultaneously each day. During the core phase of the experiment, spanning five days, mice were subjected to four trials daily. In each trial, they were released from different quadrants into the maze, with the escape platform being fixed in the first quadrant. A trial was deemed complete when a mouse successfully located the platform within a 60-second timeframe. If unsuccessful, the mouse was gently guided to the platform at the 60-second mark. The mice were handled for 10 minutes each day following the completion of the four trials.

On Day 6, a probe test was conducted to assess memory retention: the platform was removed, and mice were released from the third quadrant. The number of crossings over the previous platform location during the 60-second trial was recorded. To evaluate visual and motor function independent of spatial memory, a visible platform test was conducted on a separate cohort of control mice. The platform was made visible by placing a flag above the surface, and its location was changed between trials to prevent spatial memory. Mice underwent four trials in one day, with performance measured by latency to reach the visible platform. This design was chosen to match handling and navigation exposure, while minimizing spatial memory.

On Day 20, a second probe test was conducted using the same conditions as on Day 6, to assess long-term memory retention after a two-week interval in the home cage. Control mice underwent both the visible platform test and were subjected to identical handling procedures and probe test conditions on Day 6 and Day 20. This design ensured that differences observed in probe test performance reflected spatial memory rather than sensory or motor deficits. Mice designated for molecular or histological analysis were euthanized 60 minutes after the probe test began. This time point was selected based on established literature indicating that memory retrieval-related molecular signatures, such as the activation of immediate early genes and RNA modifications, occur at this time[94].

Chemical and reagents

All chemicals and reagents utilized in this study were of analytical grade. RNA was extracted using TRIzol® Reagent (15596-026, Invitrogen, Carlsbad, CA, USA) following the manufacturer's protocol. Chloroform and other general laboratory chemicals were obtained from Merck (109634, Darmstadt, Germany). The ACQUITY

1076 HSS T3 column (2.1×100 mm, 1.8 μm) for LC-MS/MS analysis was purchased from
1077 Waters Corporation (186008499, Milford, MA, USA). Phosphodiesterase was obtained
1078 from Sigma (P3243-1VL, St. Louis, MO, USA). Nuclease P1 and alkaline phosphatase,
1079 used for RNA digestion, were obtained from Takara (2410A and 2250A).
1080 Hydroxylamine was from Aladdin Bio-Chem Technology Co., LTD (H164487). RNase
1081 inhibitor, which is critical for preserving RNA integrity during manipulations, was
1082 purchased from New England Biolabs (M0314S, NEB, CA, USA). Methylene blue,
1083 which is used for nucleic acid visualization, was obtained from Abcam (M9140). Poly-
1084 D-lysine was purchased from Sigma (Cat No. P1149). Tamoxifen was purchased from
1085 Sigma (Cat T5648).

1086 **Subcellular fractionation**

1087 The procedure of subcellular fractionation was adapted from the methodologies in our
1088 previous studies[74,75]. Mouse brain tissues were processed starting with homogenization
1089 in Buffer A, which consists of 0.32 M sucrose, 1 mM $MgCl_2$, 1 mM PMSF, and a
1090 protease inhibitor cocktail to ensure comprehensive cell lysis while preserving protein
1091 integrity. The resultant homogenates were then filtered to remove cell debris and
1092 subsequently subjected to centrifugation at 500g for 5 minutes using a fixed-angle rotor.
1093 This step separates the homogenate into the pellet (P1) and supernatant (S1) fractions.
1094 The P1 fraction, containing primarily nuclei and unbroken cells, was further purified
1095 by resuspension in Buffer B (10 mM KCl, 1.5 mM $MgCl_2$, and 10 mM Tris-HCl at pH
1096 7.4) followed by a repeat centrifugation under the same conditions to remove any
1097 remaining debris. The final pellet was resuspended in Buffer C (20 mM HEPES, pH
1098 7.9, 25% glycerol, 1.5 mM $MgCl_2$, 1.4 M KCl, 0.2 mM EDTA, 0.2 mM PMSF, and 0.5
1099 mM DTT), which is designed for nuclear protein extraction and incubated with
1100 agitation at 4 °C for 30 minutes to facilitate the release of nuclear proteins. A final
1101 centrifugation at 12,000g for 10 minutes was performed, and the supernatant,
1102 containing the nuclear protein fraction, was collected. The initial supernatant (S1),
1103 following the removal of P1, was further centrifuged at 10,000g for 10 minutes to
1104 partition it into the P2 fraction, which included the crude synaptosomes, and the
1105 cytosolic S2 fraction.

1106 **Western blot**

1107 Homogenates of hippocampus tissue were prepared in the RIPA buffer containing 50
1108 mM Tris-HCl, pH 7.4, 150 mM NaCl, 2 mM EDTA, 1% sodium deoxycholate, 1%

1109 SDS, 1 mM PMSF, 50 mM sodium fluoride, 1 mM sodium vanadate, 1 mM DTT, and
1110 protease inhibitors cocktails. All the protein samples were boiled at 100 °C water bath
1111 for 10 minutes before western blot. Homogenates were resolved on SDS/PAGE and
1112 then transferred to nitrocellulose membranes, which were incubated in the TBS buffer
1113 (0.1% Tween-20 and 5% milk) for 1 hour at room temperature followed by incubation
1114 of primary antibodies overnight at 4 °C. After washing, the membranes were incubated
1115 with HRP-conjugated secondary antibody in the same TBS buffer for 2 hours at room
1116 temperature. Immunoreactive bands were visualized by ChemiDocTM XRS + Imaging
1117 System (BIO-RAD) using enhanced chemiluminescence (Pierce) and analyzed with
1118 Image J (NIH). The following primary antibodies were used: anti-Histone H3 (1:1000,
1119 Cell Signaling, 9715), anti-SYN1 (1:1000, Cell Signaling, 2312), anti-α-tubulin
1120 (1:10000, Cell Signaling, 3873), anti-NAT10 (1:1000, Abcam, ab194297), anti-Acetyl-
1121 Histone H3 (1:1000, Cell Signaling, 9649), anti-ARC (1:1000, Proteintech, 66550-1-
1122 Ig), anti-PSD95 (1:1000, Cell Signaling, 3450), anti-PCAF (1:1000, Cell Signaling,
1123 3378), and anti-GAPDH (1:5000, Abways, ab0037). The following secondary
1124 antibodies were used: HRP-conjugated secondary antibody (goat-anti-mouse, G-21040;
1125 goat-anti-rabbit, G-21234; 1:2000, Thermo Fisher).

1126 **Immunofluorescence**

1127 The mouse brains were fixed in 4% paraformaldehyde at room temperature for 1 hour
1128 and dehydrated in 20% sucrose at 4 °C overnight. Then the tissues were placed in an
1129 embedding mold and frozen in OCT media at 0 °C. The embedded tissues were cut into
1130 slices with the thickness of 30 μm using a Leica microtome (CM3050S). The brain
1131 slices were permeabilized with 0.3% Triton-X 100 and 5% BSA in PBS and incubated
1132 with primary antibodies at 4 °C overnight. After washing with PBS for three times,
1133 samples were incubated with secondary antibodies for 2 hours at room temperature.
1134 Samples were mounted with Vectashield mounting medium (Vector Labs) and images
1135 were taken by Leica TCS SP8 confocal microscope. The following primary antibodies
1136 were used: rabbit anti-NeuN (1:1000, Abcam, ab177487), rabbit anti-Neurogranin
1137 (1:500, Abcam, ab217672), rabbit anti-Cre (1:500, CST, 15036S), mouse anti-GFAP
1138 (1:1000, Millipore, MAB360), mouse anti-NeuN (1:1000, Abcam, ab104224). The
1139 following secondary antibodies were employed: Rabbit IgG (H+L) Highly Cross-
1140 Adsorbed Secondary Antibody (A32732, 1:500, Thermo Fisher). Unbiased stereology
1141 TissueFAX Plus ST (Tissue Gnostics, Vienna, Austria) was applied to count the

1142 number of Nat10-positive neurons. The detailed methods for cell number counting are
1143 available on the website (https://tissuegnostics.com/products/single-cell-
1144 analysis/tissuequest).

1145 **Detection of ac4C and m6A modifications by LC-MS/MS**

1146 1 μg of total RNA or polyA RNA was digested by 4 μl of nuclease P1 in 40 μl buffer
1147 (10 mM Tris-HCl, pH 7.0, 100 mM NaCl, 2.5 mM $ZnCl_2$) at 37°C for 12 hours,
1148 followed by incubation with 1 μl of alkaline phosphatase at 37°C for 2 hours. The RNA
1149 solution was then diluted to 100 μl and analyzed by LC-MS/MS. The separation of
1150 nucleosides was accomplished by means of an Agilent C18 column, and detection was
1151 achieved by AB SCIEX QTRAP 5500. Standard curves were generated to reflect the
1152 linear relationship between the ac4C (or C) concentration and their peak area during the
1153 LC-MS/MS analysis. A known concentration of ac4C or C that falls into the linear
1154 range of the standard curve (i.e, the standard samples) was analyzed alongside with the
1155 testing samples. The concentration of ac4C or C in the testing samples were calculated
1156 through normalization of the peak areas from testing samples by that from standard
1157 samples. The stoichiometry levels of ac4C were determined by the ratio of
1158 concentration of ac4C to C. The same strategies were used for analysis of the
1159 stoichiometry levels of m6A.

1160 **ac4C and m6A dot-blot**

1161 The total RNA of mouse hippocampus was extracted with Trizol according to the
1162 manufacturer's instructions. The polyA RNA was then purified using the Dynabeads™
1163 polyA RNA purification kit (61006, Thermo Fisher). The dot-blot was performed
1164 according to the previous study[27]. We used 0.5 μg of polyA RNA that fall in the linear
1165 range for each blot. For each HOM replicate, we purified 0.5 μg of polyA RNA from
1166 the hippocampus of one mouse. In contrast, for each SYN replicate, we purified 0.5 μg
1167 of polyA RNA from the hippocampus of five mice. In brief, the polyA RNA was
1168 denatured at 95 °C for 5 min using a heat block, immediately kept on ice for 1 min,
1169 loaded onto Amersham Hybond-N+ membrane and crosslinked with UV254 for 30 min.
1170 The membranes were blocked with 5% nonfat milk for 2 h at room temperature (RT),
1171 and incubated with the rabbit anti-m6A (1:2000, Synaptic System, #202003) or anti-
1172 ac4C antibody (1:500, Abcam, ab252215) at 4°C overnight. After wash with 0.05%
1173 PBST for three times, the membranes were incubated with the HRP-conjugated
1174 secondary antibody (goat-anti-rabbit, G-21234, 1:2000, Thermo Fisher) at RT for 2 h.

The signals were visualized by ChemiDocTM XRS + Imaging System (BIO-RAD) using ECL and analyzed with Image J (NIH). RNA loading was verified by staining the membranes with 0.2% methylene blue. The intensity of each dot was normalized to total RNA.

Primary neuronal culture

The primary culture of mouse hippocampal neurons was performed according to our previous studies[95]. Hippocampal explants from embryonic day 16 (E16) mouse embryos were digested with 0.125% trypsin solution for 30 min at 37°C, followed by trituration with pipette in plating medium (DMEM with 10% fetal bovine serum, 10% F-12, and 1% penicillin-streptomycin). The dissociated neurons were plated onto poly-D-lysine-coated coverslips at a density of 1×10^5 cells per 35 mm dish. Following a 4-hour incubation period, the plating medium was replaced with Neurobasal™ medium (Thermo Fisher, 21103049) supplemented with 2% B-27™ (Thermo Fisher, 17504044), 1% GlutaMax™ (Thermo Fisher, 35050061), and 1% penicillin-streptomycin (Invitrogen). Cytarabine (Sigma, C1768-100MG) was added after 2 days to a final concentration of 1 μM, to inhibit the proliferation of dividing non-neuronal cells. Half volume of the culture medium was replaced every 3-4 days with freshly prepared medium. The neurons were harvested at 14 days in vitro (DIV 14) for immunofluorescence experiments.

Chemical LTP (cLTP) and immunofluorescence

For cLTP, neurons were incubated with 300 μM glycine in a cell incubator set at 37°C with 5% CO_2 and 95% humidity for 3 minutes, followed by an additional 60 minutes without glycine at 37°C [96]. Neurons were then fixed with 4% paraformaldehyde for 30 minutes on ice to preserve cell membranes. After washing with PBS, the neurons were penetrated with 0.3% Triton-X100 and blocked with 1% BSA in PBS for 30 min at RT. After that, neurons were incubated with primary antibodies (chicken anti-MAP2 antibody, 1:2000, Abcam, ab5392; mouse monoclonal anti-PSD95 antibody, 1:800, Abcam, ab192757; and rabbit monoclonal anti-NAT10 antibody, 1:800, Abcam, ab194297) overnight at 4°C. Neurons were then washed by PBS for three times before incubation with fluorescent secondary antibodies for 2 hours at 37°C. The following secondary antibodies were employed: Chicken IgY (H+L) Secondary Antibody (A-11039, 1:500, Thermo Fisher), Rabbit IgG (H+L) Cross-Adsorbed Secondary Antibody (A-21244, 1:500, Thermo Fisher), Rabbit IgG (H+L) Highly Cross-Adsorbed

1208 Secondary Antibody (A32732, 1:500, Thermo Fisher), and Mouse IgG (H+L) Highly
1209 Cross-Adsorbed Secondary Antibody (A32727, 1:500, Thermo Fisher). After washing
1210 with PBS, the neurons were placed on mounting solution with DAPI (Beyotime, P0131).
1211 Confocal stacks were acquired from 3-6 individual fields on multiple coverslips per
1212 culture using a Leica SP8 confocal microscope. Two independent cultures were
1213 analyzed for each condition, including vehicle-treated control and glycine-treated
1214 neurons.

1215 **Regular acRIP-seq for HOM**

1216 The acRIP-seq was performed following the previous studies[19,97]. The total RNA was
1217 extracted from the HOM of mouse hippocampus using TRIzol, the quality of the RNA
1218 was evaluated through gel electrophoresis in order to ascertain its integrity and purity,
1219 and the concentration and purity of the RNA were detected. Total RNA samples,
1220 initially 100 μg, were treated with the rRNA depletion kit (New England Biolabs, Cat.
1221 No. E6310) to remove rRNA. After rRNA depletion, the RNA was subjected to
1222 immunoprecipitation using the anti-ac4C antibodies and the ac4C RIP kit (GenSeq, Cat
1223 No. GS-ET-005) according to the manufacturer's instructions. Briefly, total RNAs were
1224 randomly fragmented to ~200 nt by RNA Fragmentation Reagents (NEB, Cat No.
1225 M0348S). Protein A/G Dynabeads (Share-Bio, SB-PR001) were coupled to the anti-
1226 ac4C antibody by rotating at room temperature for 1 h. The RNA fragments were then
1227 incubated with the beads-linked anti-ac4C antibodies (2 μg) in the 100 μl acRIP buffer
1228 (PBS containing 1% Triton X-100, 2 mM BSA, and 1 mM RNase inhibitor) and rotated
1229 at 4°C for 4 h. After incubation, the RNA/antibody complexes were washed for four
1230 times with the acRIP buffer, and then RNAs were eluted by elution buffer (containing
1231 0.1 M Glycine, 0.5% Triton X-100, PH 2.5-3.1) at room temperature for 10 minutes.
1232 Finally, add NaOH solution to adjust the pH of the elution product to neutral. Both the
1233 immunoprecipitated RNA and 1% input RNA are reverse transcribed with random
1234 hexamers, followed by RNA library preparation with Ultra™ II Directional RNA
1235 Library Prep Kit (New England Biolabs, Cat No. E7760) according to the
1236 manufacturer’s instructions.

1237 The quality of RNA libraries was assessed using Agilent 2100 bioanalyzer and then
1238 subjected to the next-generation sequencing through the NovaSeq 6000 platform
1239 (Illumina). The quality of the sequencing data is measured using Q30 scores, and low-
1240 quality reads and 3' adaptors are removed using Cutadapt (v1.9.3). High-quality reads

are then aligned to the reference genome using Hisat2 (v2.0.4). Raw counts are generated using HTSeq (v0.9.1) and normalized using edgeR (v3.16.5). Gene expression was quantified by logged transcript per million mapped reads (log_2TPM) (with a cutoff TPM >1). The ac4C peaks and mRNAs that were identified from at least two of the three biological replicates of HOM were considered reliable.

Low-input acRIP-seq for SYN

The low-input acRIP-seq included some modifications, compared with the regular acRIP-seq. First, the RNA amount is relatively smaller (~ 2 μg, purified from the hippocampus of 10 mice) for low-input acRIP-seq, compared with regular acRIP-seq (~ 100 μg, purified from the hippocampus of 2 mice). Second, the total RNA purified from the SYN was not treated by the rRNA depletion kit before acRIP to avoid the non-specific RNA loss during the rRNA depletion process. Third, the RNA libraries for low-input acRIP-seq were generated by a different kit - SMARTer Stranded Total RNA-Seq Kit v2-Pico Input Mammalian (Takara, Cat No. 634413). To increase the data reliability for low-input acRIP-seq, transcripts that were identified in our own sequencing and at least two of the three synaptosome databases[43-45] were considered reliable and included in the analysis. Considering the principle of 3Rs (replacement, reduction and refinement) for animal ethics, we used one biological replicate for each time point from control and memory mice, but each replicate consists of SYN RNA purified from 10 mice. The mitochondrially encoded mRNAs and long non-coding RNA (lncRNA) were filtered out before analysis of the acRIP-seq data since the current study focused on ac4C of regular mRNA in the SYN.

Identification of ac4C peaks

Following RNA integrity assessments, acRIP enrichment verification, and library quality checks, raw sequencing reads from both acRIP and input samples underwent rigorous quality control. Initially, sequencing quality was evaluated using Q30 scores and FastQC to ensure base-level accuracy. Low-quality reads and 3' adaptor sequences were identified and removed using Cutadapt software (v1.9.3), resulting in high-quality clean reads for further analysis.

Post-alignment filtering was applied to exclude reads that mapped to mitochondrial DNA (chrM) and non-concordant mate pairs, which often arise from sequencing artifacts or alignment errors. The remaining clean reads were then aligned to the mouse genome (mm10) using Hisat2 software (v2.0.4), with parameters allowing a maximum

of five mismatches per read to ensure alignment accuracy above 95%. Ensembl gene annotations (Release 75) were incorporated to guide accurate mapping to annotated regions. To account for transcript variability, canonical transcript sequences from the UCSC genome browser were used to generate a Bowtie2 index, enabling transcriptome mapping. Reads were aligned in local mode, which is well-suited for fragmented RNA sequences.

Acetylation peaks (ac4C peaks) were identified using MACS software (v1.4.2)[98], optimized for transcriptomic data. The shifting model and local lambda options were disabled to accommodate the unique characteristics of transcriptome data, and the genome size was set according to the total transcript base count. Input samples were used as controls to distinguish true ac4C-enriched peaks from background noise. The fold enrichment (FE) of ac4C peak was calculated though the MACS software by normalizing the read counts of acRIP ac4C peak to that of input ac4C peak. We established strict screening criteria in the peak calling process: adjusted $P < 0.05$ and $FE > 2$. The adjusted p-value was acquired by MACS software using a Poisson distribution model after posthoc Benjamini-Hochberg analysis. The ac4C peaks were generated on the UCSC genome browser (https://genome.ucsc.edu/cgi-bin/hgGateway) using the IGV software (http://www.igv.org/).

Sequence motif analysis

Sequence motifs were identified using HOMER[99] and visualized using ggseqlogo package from R software. HOMER identifies motifs that are specifically enriched on memory set of sequences relative to control (e.g., peaks upstream and downstream sequences relative to the entire genome sequence) based primarily on the principle of ZOOPS scoring with hypergeometric enrichment.

Gene ontology and functional category analysis

Gene ontology (GO) analysis to detect enrichment for GO terms in differential acetylation genes in R using the clusterProfiler[100], and the possible roles of these differential acetylation genes were annotated according to MF, BP and CC. GO terms with a false-discovery rate adjusted P.adj of < 0.05 were visualized using R scripts to plot. The R package clusterProfiler to visualize the genes composing KEGG pathways, and $P.adj < 0.05$ was used as the threshold of significant enrichment.

Analysis of ac4C fold enrichment (FE) for individual mRNA

The FE of ac4C mRNA was reflected by the summary FE values of all ac4C peaks

identified in the entire transcript including the 5'UTR, CDS and 3'UTR. Averaging the cumulative distribution of these peaks offers a more comprehensive overview of the abundance of ac4C modifications across the mRNA molecule, avoiding the artificial increase of FE of long mRNAs[101]. Additionally, in instances where ac4C modifications on mRNA are more dispersed or present in low abundance, a single prominent peak may not be observable; instead, multiple low-abundance peaks might emerge. In such scenarios, the accumulation of multiple peaks can enhance detection sensitivity, better capture dynamic changes, and mitigate biases inherent in individual experiments.

$$FE\ of\ ac4C = \Sigma peak\ (1 + 2 + 3 \ldots\ldots + n)$$

Analysis of ac4C fold change (FC) for individual mRNA

The fold change of ac4C mRNA is representative of the degree of change in the overall acetylation level of mRNA in the memory group (M) compared with the control group (C). To prevent a value of 0 in the denominator in the FC calculation, we added 1 to the FE of ac4C. The FC of ac4C mRNA was calculated using the following quantification index:

$$FC\ of\ ac4C = \frac{(FE\ of\ ac4C + 1)\ in\ M}{(FE\ of\ ac4C + 1)\ in\ C}$$

Analysis of PPI network

The STRING (https://string-db.org/) (version 12.0) knowledge base was used to create a protein-protein interaction (PPI) network. The PPI network was generated with a confidence score of 0.7 and visualized using Cytoscape (version 3.10.1). Molecular Complex Detection (MCODE) (v2.0.3) algorithm was employed to identify the components of the densely connected network.

The following software and algorithms were used for the quantification and statistical analysis of ac4C epitranscriptome.

Software and algorithms, application, authors		
R v4.3.2	Statistical computing and graphics.	R Core Team. R Foundation for Statistical Computing 2023.
Python v3.11	Object-oriented programming language.	Van R et al. CreateSpace 2009.
ggplot2	Creating graphics, based on The Grammar of Graphics.	Hadley W et al, Springer-Verlag New York 2016.
ggseqlogo	Generating publication-ready	Wagih et al. Bioinformatics

	sequence logos using ggplot2.	2018.
tidyverse	Collection of R packages designed for data science.	Wickham et al. Journal of Open Source Software 2019.
ComplexHeatmap	Arrange multiple heatmaps and supports annotation graphics.	Gu Z et al. Bioinformatics 2016.
HOMER v4.11	Motif Discovery and gene sequencing analysis.	Heinz S et al. Mol Cell 2010.
bedtools	Compare large sets of genomic features.	Aaron Q et al. Bioinformatics 2010.
cutadapt v1.9.3	Remove sequencing data adaptor.	Martin M. EMBnet 2011.
Hisat2 v2.04	Mapping sequencing reads to a single reference genome.	Zhang Y et al. Genome Research 2021.
MACS v1.4.2	Identifying transcript factor binding sites.	Yong Z et al. Genome Biology 2008.
Pandas v2.1.4	Cleaning data.	The pandas development team. Zenodo 2020.
IGV	Interactive genome visualization application.	James T et al. Bioinformatics 2023.
HTSeq (v0.9.1)	Analysing high-throughput sequencing data.	Simon A et al. Bioinformatics 2014.
edgeR (v3.16.5)	Empirical analysis of digital gene expression data.	McCarthy DJ et al. Nucleic Acids Research 2012.
CIBERSORT	Cell-type identification by estimating relative subsets of RNA transcripts.	Aaron M et al. Nature methods 2015.

Identification of relative abundance of gene expression in different cell types

To determine the cellular origin of the ac4C mRNAs, we performed a bioinformatic deconvolution analysis using the CIBERSORT algorithm[102]. CIBERSORT is a computational method that uses a set of reference gene expression signatures to estimate the relative proportions of different cell types within a bulk RNA-sequencing dataset. This analysis is based on a machine learning approach, specifically ν-support vector regression (ν-SVR), which is robust against noise and confounding factors present in

complex tissue samples. The analysis first required the construction of a high-quality reference signature matrix containing the gene expression profiles of pure cell populations. We constructed this matrix using a publicly available single-cell RNA-sequencing dataset of the adult mouse hippocampus from the McCarroll Lab (http://dropviz.org/) [64].From this dataset, we extracted the expression signatures for four major hippocampal cell types: excitatory neurons, inhibitory neurons, astrocytes, and microglia, creating a signature matrix that reflects the unique transcriptomic profiles of these cells. Three groups of ac4C mRNAs (520 NAT10-independent MISA mRNAs, 717 NAT10-dependent MISA mRNAs, and 2629 NASA mRNAs that are not belong to MISA) were served as the input "mixture" file for this analysis. We then ran the CIBERSORT algorithm in R, using our custom reference signature matrix to deconvolve the NASA mRNA list. The algorithm was run with 100 permutations to ensure statistical significance of the deconvolution results. The output of CIBERSORT provides an estimation of the relative contribution of each reference cell type to the total expression of the input gene set, which allowed us to infer which cell types were the primary contributors to the three groups of ac4C mRNAs.

RT-qPCR

The cDNA was obtained through reverse transcription using the HiScript III RT SuperMix for qPCR kit (Vazyme, R323-01), followed by amplification using the ChamQ Universal SYBR qPCR Master Mix kit (Vazyme, Q711-02). Gene expression levels measured with RT-PCR were normalized to Gapdh. The primers used in qPCR for this study were as follows: Gapdh-forward, 5’gggtgtgaaccacgagaaat3’; Gapdh-reverse 5’actgtggtcatgagcccttc3’; Arc-forward, 5’ggagggaggtcttctaccgtc3’; Arc-reverse 5’cccccacacctacagagaca3’; Grin2b-forward, 5’ctggtgaccaatggcaagcatg3’; Grin2b-reverse, 5’ggcacagagaagtcaaccacct3’; Camk2α-forward, 5’agccatcctcaccactatgctg3’; Camk2α-reverse 5’gtgtcttcgtcctcaatggtgg3’.

Stereotaxic injection of AAV into mouse hippocampus

AAV2/9-Syn1-EGFP and AAV2/9-Syn1-EGFP-P2A-Cre were generated by Hanbio Technology (Shanghai) Corp., Ltd., with a titer of 10^{12}/μl. We injected 0.3 μl AAV into each side of the mouse hippocampus. Six-week-old $Nat10^{flox/flox}$ mice received an intraperitoneal injection of alphaxalone at a dosage of 40 mg/kg for anesthesia and then were immobilized in a stereotaxic frame provided by RWD Life Science. Similarly, AAV2/9-CAG-DIO-EGFP, generated by Hanbio Technology (Shanghai) Corp., Ltd.,

with a titer of 10^{12}/μl, was injected into the hippocampus of seven-week-old Nat10$^{Cre/+}$ mice. The AAVs were delivered into mouse hippocampus through a stereotaxic injector at a flow rate of 0.1 μl/min. The precise coordinates for the stereotaxic injection were set to anteroposterior (AP) −2.3 mm, dorsoventral (DV) −1.8 mm, and mediolateral (ML)±1.75 mm, relative to the Bregma. To induce Cre enzyme expression, mice were fed a custom-made tamoxifen-infused diet over a period of one week[103].

Electrophysiological recording

Hippocampal slices were prepared as previously described[104]. Briefly, mice (10 weeks old, male) were decapitated and transverse hippocampal slices (400 μm) were prepared using a Vibroslice (VT 1000S; Leica) in ice-cold ACSF. For field potential recording, the same ACSF was used for slice preparation and recording: 120 mM NaCl, 2.5 mM KCl, 1.2 mM NaH_2PO_4, 2.0 mM $CaCl_2$, 2.0 mM $MgSO_4$, 26 mM $NaHCO_3$ and 10 mM glucose. After sectioning, hippocampal slices were allowed to recover in the chamber for 30 min at 34°C and then for a further 2-8 h at room temperature (25 ± 1°C). All solutions were saturated with 95% O_2/5% CO_2 (vol/vol).

The slices were placed in the recording chamber, which was superfused (3 mL/min) with ACSF at 32-34°C. fEPSPs were evoked in the CA1 stratum radiatum by stimulating the SC with a bipolar stimulating electrode (FHC) and recorded in current clamp using a HEKA EPC 10 amplifier (HEKA Elektronik) with ACSF-filled glass pipettes (1-3 MΩ). Test stimuli consisted of monophasic 100-μs pulses of constant current (intensity adjusted to produce 25% of the maximum response) at a frequency of 0.033 Hz. The strength of synaptic transmission was determined by measuring the initial amplitude of fEPSPs. L-LTP was induced by 4 trains of 100 Hz stimuli of 50 pulses each at 100 Hz, 10 s apart, at the same intensity as the test stimulus. The level of E-LTP / L-LTP was determined at an average of 55-60 / 115-120 min after HFS stimulation. To study glutamatergic transmission at SC-CA1 synapses, we recorded fEPSP input/output (I/O) curves at SC-CA1 synapses. To construct an I/O curve, fEPSPs were evoked by a series of incremental intensities (0.02-0.2 mA in 0.02 mA increments, 100 μs duration, at 0.033 Hz). Whole-cell patch-clamp recordings from CA1 neurons were visualized with infrared optics using an upright microscope

equipped with a 40× water-immersion objective (BX51WI; Olympus) and an infrared-sensitive CCD camera. To analyze the intrinsic excitability of CA1 pyramidal neurons, the current clamp was used and neurons were held at 0 pA and then injected with step currents (duration: 500 ms; increments: 20 pA; range: -100 to 400 pA; interval: 10 s). The input-output relationship was determined by plotting the injected currents against the number of action potentials. All data were acquired at a sampling rate of 10 kHz using PATCHMASTER version 2 x 90.1 software (HEKA Elektronik) and filtered off-line at 1 kHz.

Generation and use of the ac4C website

The ac4Catlas website was constructed using HTML (a scripting language for front-end development), PHP (a scripting language for backend development), and MySQL (a structured query language for data operation). All the website codes were deployed in a Linux server equipped with Centos environment. The raw data, processed data and annotated files were stored in "Data Downloads" section. JBrowse (https://jbrowse.org) was integrated to visualize the ac4C epitranscriptomic data on genomic regions of interest. Briefly, ac4Catlas provides user-friendly interactive interfaces which allow researchers to freely browse and perform extended operations, such as searching, comparing, and downloading. Besides, the browse module stores detailed information of samples and corresponding datasets as well as ac4C levels of mRNA and differentially acetylated regions between groups.

Statistical analysis

The cumulative distribution curve was analyzed by Kolmogorov-Smirnov test in R. The statistical analysis of percentage of ac4C summits occurring within CDS or UTRs was performed by chi-square test in R. The regular quantification data were shown as mean ± SEM unless otherwise mentioned. The sample size justification was based on the previous studies and met the requirement of statistics power. For normally distributed data with 1 experimental variable, statistical analyses were performed by parametric analysis: unpaired (two-tailed) student's t-test for two groups and one-way ANOVA with the Tukey's or sidak multiple-comparison test for 3 groups. Data with >1

experimental variable were evaluated by two-way ANOVA, with post hoc Tukey, Dunnett or Sidak's multiple-comparison tests. All these statistical analyses were performed by the software of GraphPad Prism 10. Statistically significant difference was indicated as follows: *** $P < 0.001$, ** $P < 0.01$ and * $P < 0.05$.

Acknowledgements

We thank CloudSeq Inc. (Shanghai, China) for providing us with technical support on acRIP-seq. This work was supported by STI2030-Major Projects (Grant No. 2021ZD0202500), National Natural Science Foundation of China (Grant No.32500917), Natural Science Foundation of Chongqing, China (Grant No. 2022NSCQ-MSX5813), and the Proton Cluster Incubation Project of the National Natural Science Foundation of China (Grant No. 2025GZRFY01).

Author contributions

H.-Q.Z. and H.J. performed biochemical and behavioral analysis, H.-Q.Z., Z.Z. and J.-W.Z. analyzed the data, W.-P.L., Y.-Y.D., and S.L. performed electrophysiology. D.-M.Y. conceived the idea, supervised the work and wrote the paper. All authors approved the final version of the manuscript.

Competing interests

The authors declare no competing interests.

Data and materials availability

All data are available in the main text, supplementary or source data files. The original data of acRIP-seq is accessible via the website (http://ac4Catlas.com/) or GEO database (GSE261922). All unique materials used are readily available from the corresponding author upon reasonable requests.

Code availability

Custom code used in this paper is available at https://github.com/YinDMlab/ac4CRIP-seq-analysis.

Figures and Legends

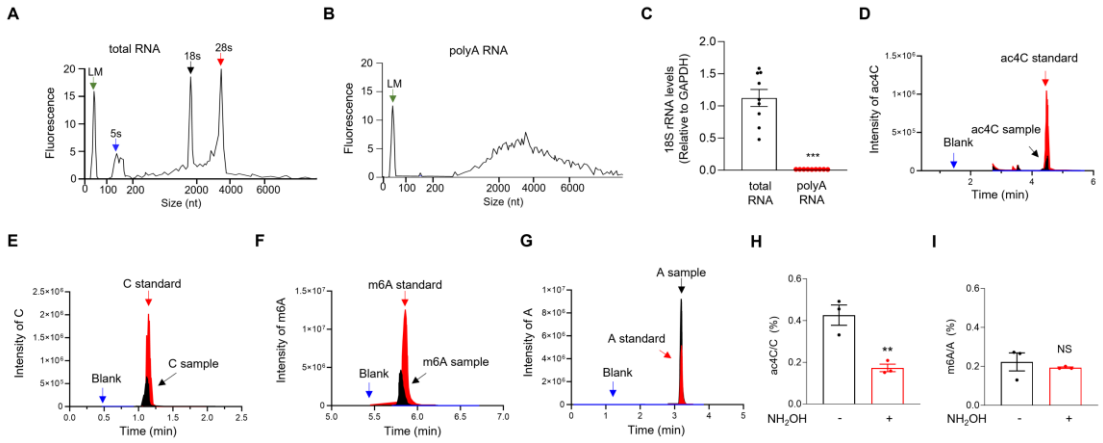

Figure 1 The presence of ac4C modification in PolyA RNA of mouse hippocampus. (A, B) Verification of the purity of PolyA RNA through the bioanalyzer profiling. The x-axis represents the size of nucleotides, and the y-axis represents the fluorescent signal from the bioanalyzer. LM, Lower Marker. (A), total RNA. (B), polyA RNA. (C) Diminished levels of 18S rRNA in the polyA RNA samples, compared with total RNA samples, which was revealed by RT-qPCR analysis. The levels of 18S rRNA were normalized by that of Gapdh. *** $P < 0.001$, two-tailed t-test, $n = 6$ biological replicates. (D-G) The chromatograms of blank, standard and testing samples of ac4C (D), C (E), m6A (F) and A (G) in the LC-MS/MS analysis. Shown are the representative peaks of ac4C, C, m6A and A identified in the polyA RNA samples purified from the HOM of mouse hippocampus. (H) Reduction of ac4C levels by the chemical deacetylation protocol. The stoichiometry levels of ac4C in polyA RNA from control and NH_2OH-treated samples were quantified. ** $P = 0.008$, two-tailed t-test, $n = 3$ biological replicates. (I) Unchanged m6A levels by the chemical deacetylation protocol. The stoichiometry levels of m6A in polyA RNA from control and NH_2OH-treated samples were quantified. NS, not significant, two-tailed t-test, $n = 3$ biological replicates. Quantification data are expressed as mean ± SEM.

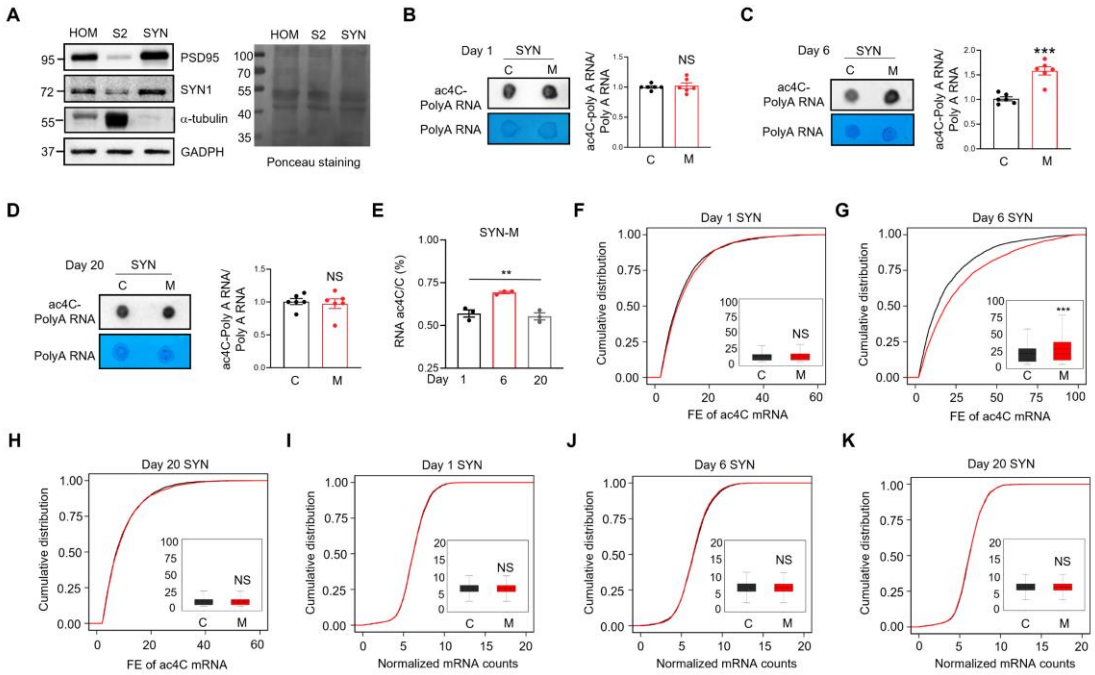

Figure 2 Increased mRNA acetylation in the SYN of mouse hippocampus after memory. (A) The purified synaptosomes (SYN) of mouse hippocampus expressed high levels of PSD95 and synapsin 1 (SYN1), two synaptic protein markers, but very low levels of α-tubulin, a cytoplasmic protein marker. The homogenates (HOM), cytoplasm (S2) and SYN of mouse hippocampus were subjected to western blots with the indicated antibodies. Left panel, representative images of western blots; right panel, Ponceau staining to show equal protein loading. **(**B) Acetylation of polyA RNA was not altered in SYN of mouse hippocampus at day 1. The polyA RNA purified from the SYN of control and memory mice at day 1 after MWM training were subjected to ac4C dot-blots and methylene blue staining. Left, the representative images; right, quantification data. NS, not significant, two-tailed t-test, n = 6 biological replicates. Data were normalized by controls. (C) Acetylation of polyA RNA was increased in the SYN of mouse hippocampus at day 6. The polyA RNA purified from the SYN of control and memory mice at day 6 after MWM training were subjected to ac4C dot-blots and methylene blue staining. Left, the representative images; right, quantification data. *** P <0.001, two-tailed t-test, n = 6 biological replicates. Data were normalized by controls. (D) Acetylation of polyA RNA was not altered in the SYN of mouse hippocampus at day 20. The polyA RNA purified from the SYN of control and memory mice at day 20

after MWM training were subjected to ac4C dot-blots and methylene blue staining. Left, the representative images; right, quantification data. NS, not significant, two-tailed t-test, n = 6 biological replicates. Data were normalized by controls. (E) Acetylation of RNA in the SYN was increased during memory but returned to normal levels after forgetting. The stoichiometry levels of ac4C of total RNA purified from the SYN of memory (M) mice were shown at days 1, 6 and 20 after MWM training. ** P = 0.0023, one-way-ANOVA, n = 3 biological replicates. (F-H) Acetylation of mRNA was increased after memory but returned to normal levels after forgetting in the SYN of mouse hippocampus. Shown are cumulative distribution curves of FE of ac4C mRNA purified from the SYN of control (C) and memory (M) mice at days 1 (F), 6 (G), and 20 (H) after MWM training. The FE of ac4C mRNA was quantified in the quartile boxplots, where the solid line in the box is the median and the dashed line is the mean, where the maximum and minimum values are identified. NS, not significant, *** adj-P = 9.9814e-13, Kolmogorov-Smirnov test. (I-K) The total mRNA levels were not significantly altered in the SYN of mouse hippocampus during memory. Shown are cumulative distribution curves of normalized mRNA counts for SYN in control (C) and memory (M) mice at days 1 (I), 6 (J) and 20 (K) after MWM training. The normalized mRNA counts were quantified in the quartile boxplots, where the solid line in the box is the median and the dashed line is the mean, where the maximum and minimum values are identified. NS, not significant, Kolmogorov-Smirnov test. C, control; M, memory. FE, Fold Enrichment. Quantification data are expressed as mean ± SEM.

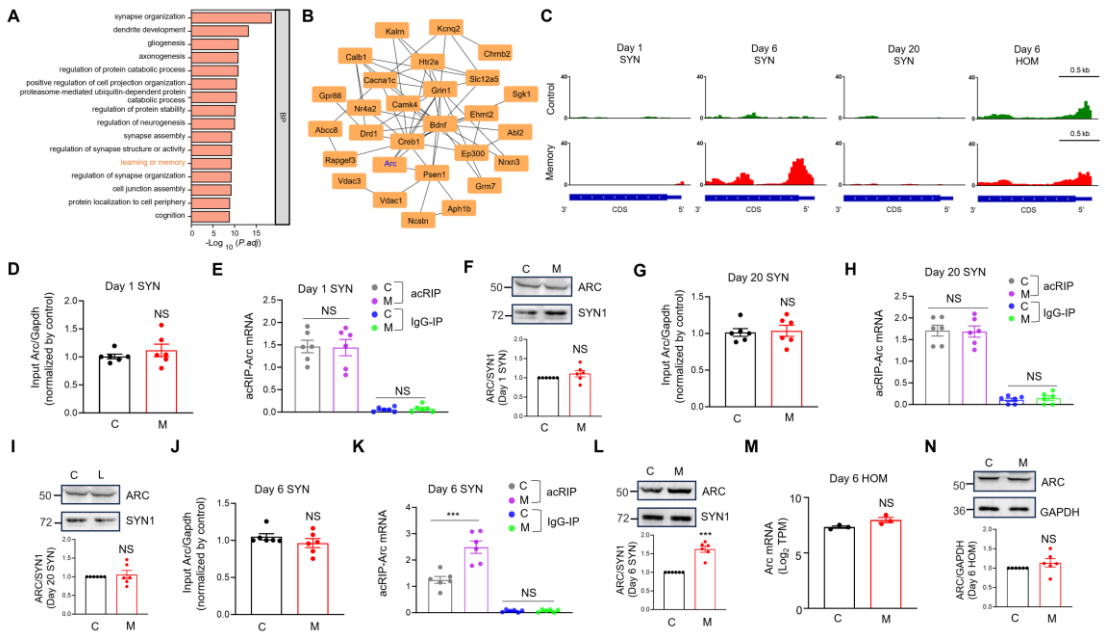

Figure 3 A representative MISA mRNA for Arc. (A) The top 16 BP in which MISA mRNAs are significantly overrepresented. The x-axis represents the negative logarithm of the adjusted p-value, reflecting the significance of the enrichment, while the y-axis shows the biological processes. (B) The protein-protein interaction (PPI) network of MISA mRNA implicated in the BP of learning or memory. P < 1.0e-16, Hypergeometric Test**.** (C) Increased ac4C modification of Arc in the SYN rather than in the HOM at day 6. Also note the unaltered ac4C Arc mRNA at days 1 or 20 in the SYN. Shown are the IGV maps of the ac4C peaks from the 3' UTR to the 5' UTR of Arc mRNA. The ac4C peaks were represented by acRIP/input (See details in the Method). (D, G) Arc mRNA levels from the input of SYN were not altered at days 1 (D) or 20 (G) after MWM training. The RNA purified from the SYN was subjected to the RT-qPCR analysis. NS, not significant, two-tailed t-test, n = 6 biological replicates. The levels of Arc mRNA were normalized by that of Gapdh in each sample, and then the ratio of Arc to Gapdh were normalized by controls. (E and H) The ac4C modification of Arc mRNA was not altered in the SYN at days 1 (E) or 20 (H) after MWM training. The RNA purified through the acRIP and IgG-IP products of SYN was subjected to the RT-qPCR analysis. NS, not significant, two-way-ANOVA followed by Tukey's multiple comparison test, n = 6 biological replicates. Data were normalized by input. (F and I**)** The protein levels of ARC did not change in the SYN at days 1 (F) or 20 (I) after MWM training. Top,

representative western blot images; bottom, quantification data. NS, not significant, two-tailed t-test, n = 6 biological replicates. The protein levels of ARC were normalized by that of SYN1 in each sample, and then the ratio of ARC to SYN1 were normalized by controls. (J) Arc mRNA levels from the input of SYN were not altered at day 6 after MWM training. The RNA purified from the SYN was subjected to the RT-qPCR analysis. NS, not significant, two-tailed t-test, n = 6 biological replicates. The levels of Arc mRNA were normalized by that of Gapdh in each sample, and then the ratio of Arc to Gapdh were normalized by controls. (K) The ac4C modification of Arc mRNA was significantly increased in the SYN at day 6 after MWM training. The RNA purified from the acRIP and IgG-IP products of SYN was subjected to the RT-qPCR analysis. *** $P < 0.001$, two-way-ANOVA followed by Tukey's multiple comparison test, n = 6 biological replicates. Data were normalized by input. (L) The protein levels of ARC were significantly increased in the SYN at day 6 after MWM training. Top, representative western blot images; bottom, quantification data. *** $P < 0.001$, two-tailed t-test, n = 6 biological replicates. The protein levels of ARC were normalized by that of SYN1 in each sample, and then the ratio of ARC to SYN1 were normalized by controls. (M) Arc mRNA levels from the HOM were not altered at day 6 after MWM training. The Arc mRNA levels were revealed by the $\log_2$TPM from the next-generation sequencing of the HOM RNA. NS, not significant, two-tailed t-test, n = 3 biological replicates. (N) The protein levels of ARC did not change in the HOM at day 6 after MWM training. Top, representative western blot images; bottom, quantification data. NS, not significant, two-tailed t-test, n = 6 biological replicates. The protein levels of ARC were normalized by that of GAPDH in each sample, and then the ratio of ARC to GAPDH were normalized by controls. C, control; M, memory. Quantification data are expressed as mean ± SEM.

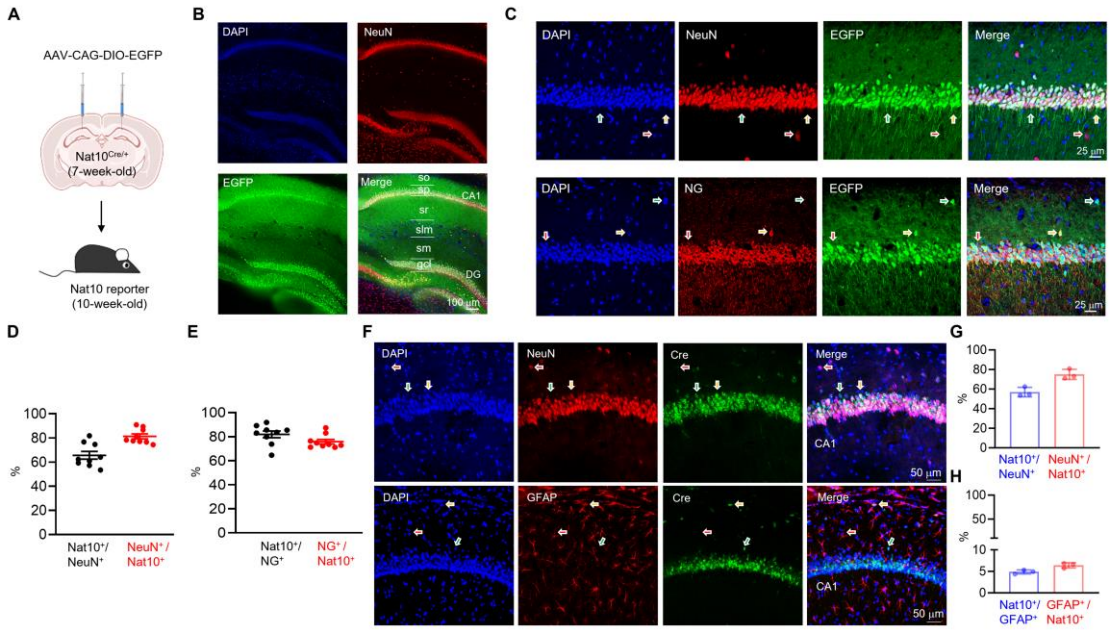

Figure 4 Expression of Nat10 in mature neurons of mouse hippocampus. (A) Experimental design. Cre-reporting AAV was injected into the dorsal hippocampus of 7-week-old Nat10$^{Cre/+}$ mice. Three weeks after AAV injection, the fluorescent protein EGFP was analyzed in the Nat10 reporter mice. (B) Co-localization of EGFP with NeuN in the hippocampus of Nat10 reporter mice. The hippocampal slices from Nat10 reporter mice were immunostained with anti-NeuN antibodies. so, stratum oriens; sp, stratum pyramidale; sr, stratum radiatum; slm, stratum lacunosum-moleculare; sm, stratum moleculare; gcl, granule cell layer; DG: dentate gyrus. Scale bar, 100 μm. (C) Co-localization of EGFP and NeuN (top) or NG (bottom) in the CA1 region of Nat10 reporter mice. The hippocampal slices from Nat10 reporter mice were immunostained with anti-NeuN or anti-NG antibodies. The yellow arrows indicate a neuron (top) or excitatory pyramidal neuron (bottom) expressing Nat10, whereas the red arrows represent a neuron (top) or excitatory pyramidal neuron (bottom) not expressing Nat10. The green arrows indicate non-neuronal cells that expresses Nat10. Scale bar, 25 μm. (D) Quantification of the percentage of Nat10-expressing neurons (Nat10$^+$ / NeuN$^+$ = 65.61 ± 3.245%) and the percentage of neurons in Nat10-positive cells (NeuN$^+$ / Nat10$^+$ = 81.31 ± 2.029%) in panel C. n = 9 slices from 3 mice. (E) Quantification of the percentage of Nat10-expressing excitatory neurons (Nat10$^+$ / NG$^+$ = 81.87 ± 2.765%) and the percentage of excitatory neurons in Nat10-positive cells (NG$^+$ / Nat10$^+$ = 75.82

± 1.882%) in panel C. n = 9 slices from 3 mice. (F) Co-localization of Cre with NeuN (top) or GFAP (bottom) in the hippocampus of $Nat10^{Cre/+}$ mice. Hippocampal sections from $Nat10^{Cre/+}$ mice were immunostained with anti-NeuN or anti-GFAP antibodies. The yellow arrows indicate a neuron (top) or astrocyte (bottom) expressing Nat10, whereas the red arrows represent a neuron (top) or astrocyte (bottom) not expressing Nat10. The green arrows indicate Nat10-positive cells not expressing NeuN (top) or GFAP (bottom). Scale bar, 50 μm. (G) Quantification of the percentage of Nat10-expressing neurons ($Nat10^{+}$ / $NeuN^{+}$ = 56.93 ± 2.795%) and the percentage of neurons in Nat10-positive cells ($NeuN^{+}$ / $Nat10^{+}$ = 75.07 ± 2.968%) in panel F. n = 3 slices from 3 mice. (H) Quantification of the percentage of Nat10-expressing astrocytes ($Nat10^{+}$ / $GFAP^{+}$ = 4.88 ± 0.273%) and the percentage of astrocytes in Nat10-positive cells ($GFAP^{+}$ / $Nat10^{+}$ = 6.39 ± 0.346%) in panel F. n = 3 slices from 3 mice.

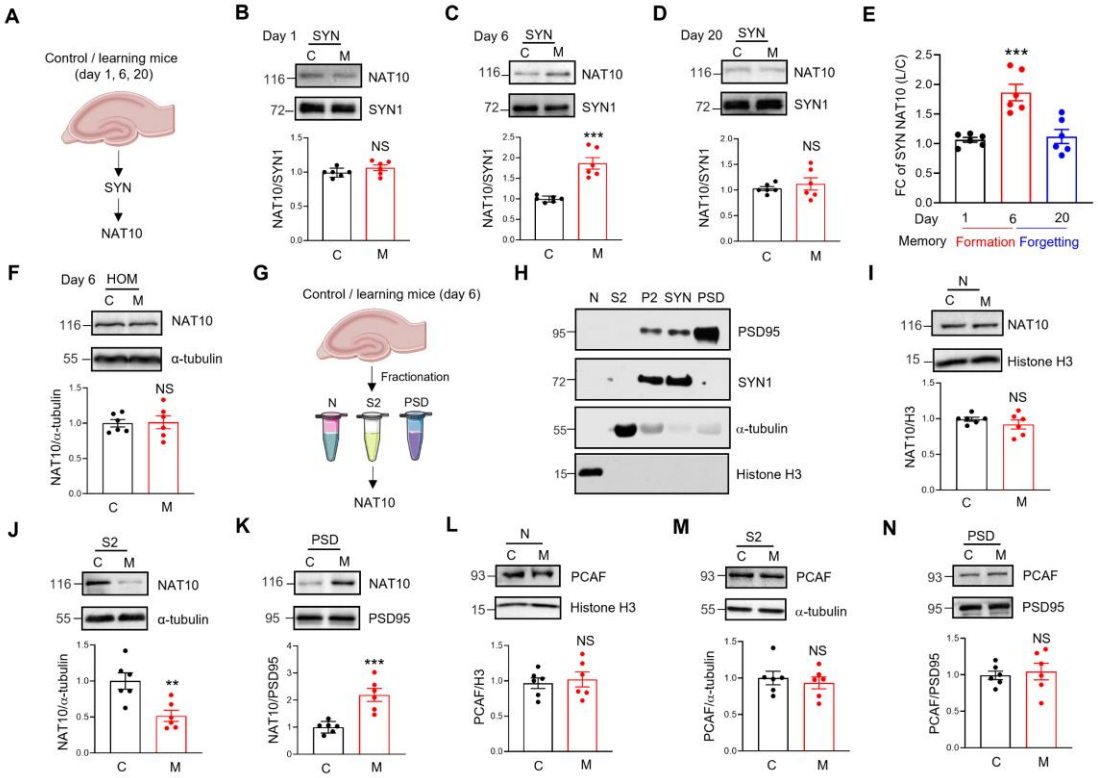

Figure 5 Increased NAT10 proteins in the SYN of mouse hippocampus after memory. (A) Experimental design. The SYN fractions were purified from the hippocampus of control and memory mice at days 1, 6 and 20. The NAT10 protein levels in the SYN were then assessed by western blots. (B-D) Protein levels of NAT10

1608 were increased in the SYN after memory but returned to normal levels after forgetting.
1609 The SYN proteins from control and memory mice at days 1 (B), 6 (C), and 20 (D) were
1610 subjected to western blots with the indicated antibodies. The protein levels of NAT10
1611 were normalized by that of SYN1 in each sample, and then the ratio of NAT10 to SYN1
1612 was normalized by controls. Top, representative western blot images; bottom,
1613 quantification data. NS, not significant, ***P < 0.001, two-tailed t-test, n = 6 biological
1614 replicates. (E) The fold change (FC) of NAT10 proteins in panel B-D was quantified.
1615 ***P < 0.001, one-way-ANOVA, n = 6 biological replicates. (F) Protein levels of
1616 NAT10 were not altered in the HOM at day 6. The HOM proteins from control and
1617 memory mice at day 6 were subjected to western blots with the indicated antibodies.
1618 Top, representative western blot images; bottom, quantification data. NS, not significant,
1619 two-tailed t-test. Data were normalized by controls, n = 6 biological replicates at each
1620 condition. The protein levels of NAT10 were normalized by that of α-tubulin in each
1621 sample, and then the ratio of NAT10 to α-tubulin was normalized by controls. (G)
1622 Experimental design. Proteins were extracted from nucleus (N), cytoplasm (S2), and
1623 postsynaptic density (PSD) of control and memory mice hippocampus at day 6, and
1624 then NAT10 protein levels were assessed by western blots. (H) Expression of different
1625 protein markers in the nuclear (N), cytoplasmic (S2), P2 (Crude synaptosomes fraction),
1626 SYN, and PSD fractions of mouse hippocampus. Shown are representative images of
1627 western blots. Protein samples purified from different subcellular fractions of mouse
1628 hippocampus were subjected to western blots with the indicated antibodies. (I) Protein
1629 levels of NAT10 were not altered in the nuclear fraction of mouse hippocampus after
1630 memory. The nuclear protein samples from control and memory mice at day 6 were
1631 subjected to western blots with the indicated antibodies. Top, representative western
1632 blot images; bottom, quantification data. NS, not significant, two-tailed t-test, n = 4
1633 biological replicates. The protein levels of NAT10 were normalized by that of Histone
1634 H3 proteins in each sample, and then the ratio of NAT10 to Histone H3 was normalized
1635 by controls. (J) Protein levels of NAT10 were significantly reduced in the S2 fraction
1636 of mouse hippocampus after memory. The cytoplasmic protein samples from control

and memory mice at day 6 were subjected to western blots with the indicated antibodies. Top, representative western blot images; bottom, quantification data. ** P = 0.0052, two-tailed t-test, n = 6 biological replicates. The protein levels of NAT10 were normalized by that of α-tubulin in each sample, and then the ratio of NAT10 to α-tubulin was normalized by controls. (K) Protein levels of NAT10 were significantly increased in the PSD fraction of mouse hippocampus after memory. The PSD protein samples from control and memory mice at day 6 were subjected to western blots with the indicated antibodies. Top, representative western blot images; bottom, quantification data. *** P = 0.0008, two-tailed t-test. n = 6 biological replicates. The protein levels of NAT10 were normalized by that of PSD95 in each sample, and then the ratio of NAT10 to PSD95 was normalized by controls. (L-N) Protein levels of PCAF were not altered in the nuclear (L), S2 (M), or PSD fraction (N) of mouse hippocampus after memory. The protein samples purified from the different subcellular fractions of the hippocampus of control and memory mice at day 6 were subjected to western blots with the indicated antibodies. Top, representative western blot images; bottom, quantification data. NS, not significant, two-tailed t-test, n = 6 biological replicates. The protein levels were normalized by the protein markers in different subcellular fractions and then were normalized by controls. C, control; M, memory. Quantification data are expressed as mean ± SEM.

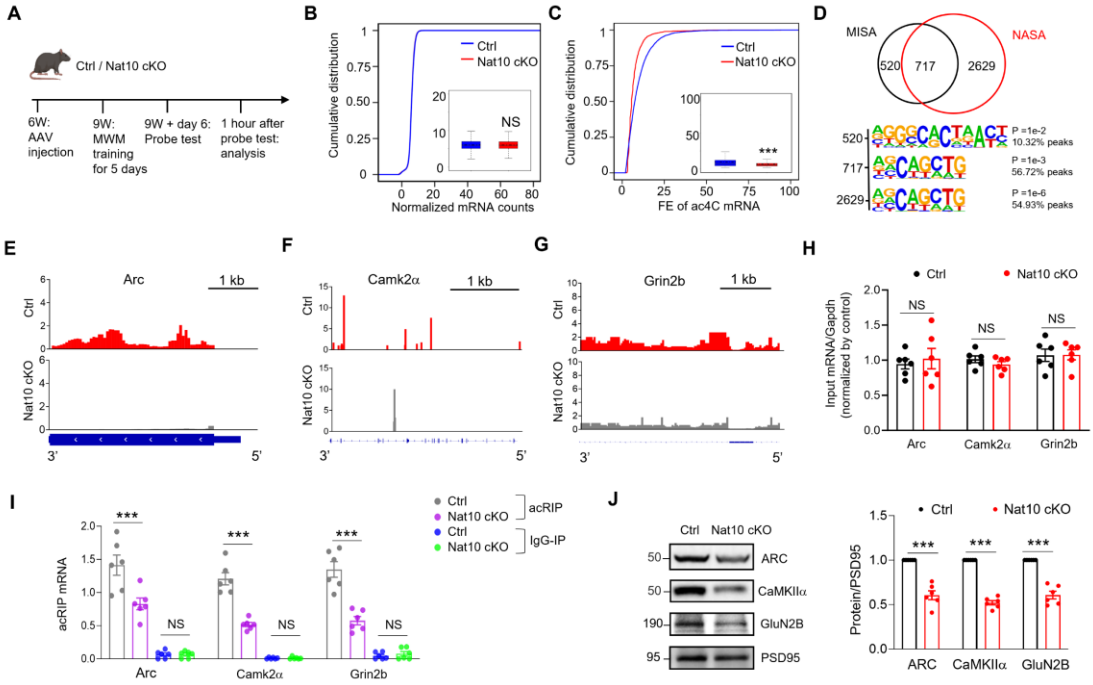

Figure 6 NAT10-dependent ac4C modification of memory-related mRNAs in the SYN of memory mice. (A) Experimental design. Three weeks after AAV injection, the control (Ctrl) and Nat10 conditional knockout (cKO) mice were subjected to MWM training and probe test, and then the SYN fractions were purified from hippocampal tissues for low-input acRIP-seq. (B) The total mRNA levels were not significantly altered in the SYN of Nat10 cKO mice, compared to controls. Shown are cumulative distribution curves of normalized mRNA counts for SYN in control and Nat10 cKO mice at day 6 after MWM training. The normalized mRNA counts were quantified in the quartile boxplots, where the solid line in the box is the median and the dashed line is the mean, where the maximum and minimum values are identified. NS, not significant, Kolmogorov-Smirnov test. (C) Acetylation of mRNA in the SYN of Nat10 cKO mice was significantly reduced, compared with controls. Shown are cumulative distribution curves of FE of ac4C mRNA purified from the SYN of control and Nat10 cKO mice at day 6 after MWM training. The FE of ac4C mRNA was quantified in the quartile boxplots, where the solid line in the box is the median and the dashed line is the mean, where the maximum and minimum values are identified. *** adj-P = 1.20076e-12, Kolmogorov-Smirnov test. (D) Venn diagrams show overlapping between MISA mRNA and NASA mRNA. Distinct consensus motifs distinguish NAT10-

dependent and NAT10-independent MISA mRNAs. Sequence motif analysis reveals fundamentally different consensus sequence patterns between the two MISA mRNA populations identified in the Venn diagram. (E-G) Reduced ac4C modification of Arc (E), Camk2α (F), and Grin2b (G) mRNA in the SYN of Nat10 cKO mice at day 6, compared with controls. Shown are the IGV maps of the ac4C peaks from the 3' UTR to the 5' UTR of transcripts. The ac4C peaks were represented by acRIP/input (See details in the Method). (H) The mRNA levels of Arc, Camk2α and Grin2b from the input of SYN were similar between control and Nat10 cKO mice. The RNA purified from the SYN was subjected to the RT-qPCR analysis. NS, not significant, two-tailed t-test, n = 6 biological replicates. The levels of mRNA were normalized by that of Gapdh in each sample, and then the ratio of mRNA to Gapdh were normalized by controls. (I) The ac4C modification of Arc, Camk2α, and Grin2b mRNA was significantly reduced in the SYN of Nat10 cKO mice at day 6, compared with controls. The RNA purified from the acRIP and IgG-IP products of SYN was subjected to the RT-qPCR analysis. *** $P < 0.001$, two-way-ANOVA followed by Tukey's multiple comparison test, n = 6 biological replicates. Data were normalized by input. (J) The protein levels of ARC, CaMKIIα and GluN2B were significantly decreased in the SYN of Nat10 cKO mice at day 6, compared with controls. Left, representative western blot images; right, quantification data. *** $P < 0.001$, two-tailed t-test, n = 6 biological replicates. The protein levels were normalized by that of PSD95 in each sample, and then the ratio of protein to PSD95 were normalized by controls. Quantification data are expressed as mean ± SEM.

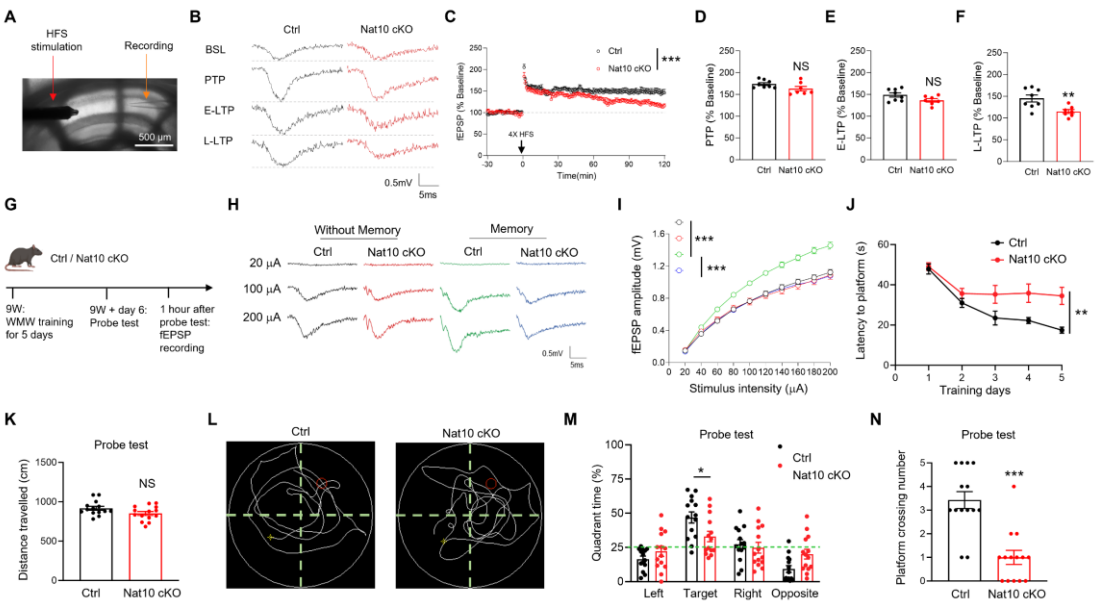

Figure 7 Impaired LTP as well as memory in the Nat10 cKO mice. (A) A representative image showing recording LTP at the SC-CA1 synapses from Nat10 cKO mice using the protocol of high-frequency stimulation (HFS). Scale bar, 500 μm. (B) The representative fEPSP traces from baseline (BSL), post-tetanus potentiation (PTP), early phase of LTP (E-LTP, 55-60 min after HFS) and late phase of LTP (L-LTP, 115-120 min after HFS). (C) Impaired maintenance of L-LTP at the SC-CA1 synapses in Nat10 cKO mice, compared with controls. Normalized fEPSP amplitudes were plotted every 1 min for hippocampal slices from control and Nat10 cKO mice. *** $P < 0.001$, two-way ANOVA, n = 8 slices from 4 mice for each group. (D) Normal LTP induction at the SC-CA1 synapses in Nat10 cKO mice, compared to controls. The PTP in panel C was quantified. NS, not significant, two-tailed t-test. n = 8 slices from 4 mice for each group. (E) Unaltered E-LTP at the SC-CA1 synapses in Nat10 cKO mice, compared to controls. The E-LTP in panel C was quantified. NS, not significant, two-tailed t-test. n = 8 slices from 4 mice for each group. (F) Impaired L-LTP at the SC-CA1 synapses in Nat10 cKO mice, compared with controls. The L-LTP in panel C was quantified. ** $P = 0.008$, two-tailed t-test. n = 8 slices from 4 mice for each group. (G) Experimental design. The control and Nat10 cKO mice were subjected to fEPSP recording at the SC-CA1 synapses after training and probe test in the MWM. (H, I) Memory-induced enhancement of glutamatergic transmission at SC-CA1 synapses was significantly

impaired in Nat10 cKO mice, compared with controls. (H) Representative fEPSP traces from control and Nat10 cKO mice. (I) Quantification of the fEPSP amplitudes in panel H. *** Genotype $F_{(3, 680)} = 128.2$, $P < 0.001$, two-way ANOVA followed by Sidak's multiple comparison test, n = 18 slices from 5 mice each group. (J) Impaired memory process in Nat10 cKO mice, compared with controls. Shown are the memory curves of control and Nat10 cKO mice in the MWM. n = 14 mice per group, ** Genotype $F_{(1, 130)} = 24.08$, ** $P = 0.0014$, two-way ANOVA followed by Sidak's multiple comparison test. (K) Similar distance travelled during probe tests between control and Nat10 cKO mice. NS, not significant, two-tailed t-test, n = 14 mice per group. (L) Representative swimming traces of control and Nat10 cKO mice during probe tests. (M) Time spent in the target quadrant was significant reduced in Nat10 cKO groups during probe tests, compared with controls. * $P = 0.0198$, two-way ANOVA followed by Sidak's multiple comparison with post hoc t-test, n = 14 mice per group. (N) Number of platform crossing was significantly reduced in Nat10 cKO mice during probe tests, compared with controls. *** $P < 0.001$, two-tailed t-test, n = 14 mice per group. Quantification data are expressed as mean ± SEM.

Supplementary Figures

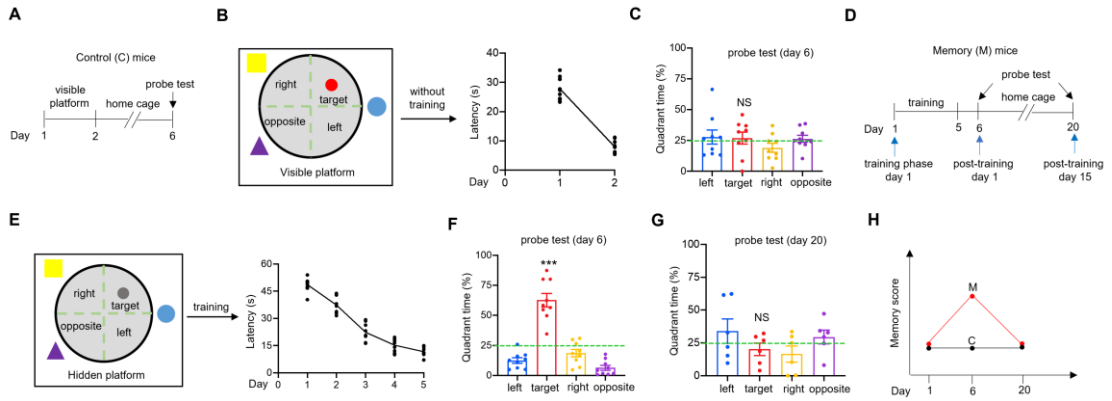

Supplementary Figure 1 Protocols of MWM for control and memory mice. (A) MWM protocol for control mice. The control mice were placed in MWM with a visible platform at day 1 and 2, after which they returned to home cage and were subjected to probe tests at day 6. (B) Control mice were able to discern the visible platform above

the water surface and consequently locate it rapidly. Shown are the latency to find the visible platform at day 1 and 2. (C) Control mice were not able to remember the target quadrant during probe tests on day 6. Shown are the percentage of time staying in each quadrant during probe tests. n = 9 mice, NS, not significant, one-way ANOVA. (D) MWM protocol for memory mice. The memory mice were trained in MWM with a hidden platform from day 1 to 5 (i.e. training phase day 1 to 5), and then were subjected to probe tests at day 6 (i.e., post-training day 1) and 20 (i.e., post-training day 15). (E) Memory mice showed improvement in their ability to find the hidden platform during the training process. Shown are the memory curves. (F) Memory mice could remember the target quadrant during probe tests at day 6. Shown are the percentage of time staying in each quadrant during probe tests. n = 9 mice, *** P < 0.001, one-way ANOVA. (G) Memory mice could not remember the target quadrant during probe tests at day 20. Shown are the percentage of time staying in each quadrant during probe tests. n = 6 mice, NS, not significant, one-way ANOVA. (H) Schematic summary of memory score of control and memory mice at day 1, 6, and 20 after MWM training. Memories were recalled at day 6 but were forgotten at day 20 in memory mice. The memory score indicates spatial memory performance in the MWM test.

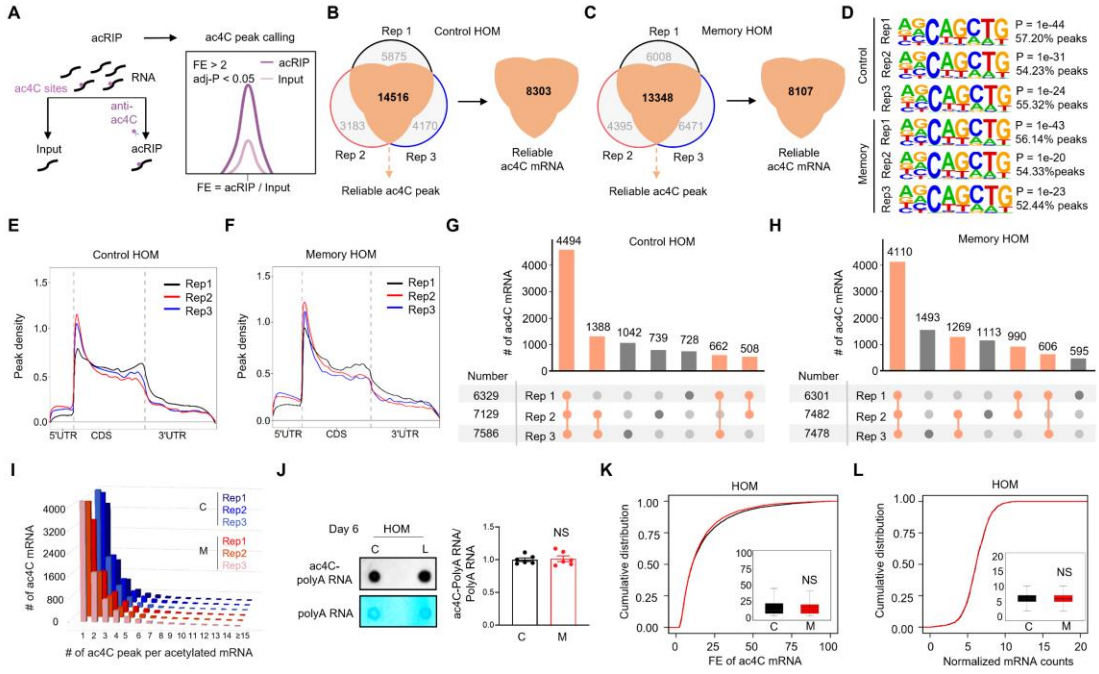

Supplementary Figure 2 No significant change of ac4C mRNA in the homogenates of mouse hippocampus after memory. (A) Experimental design. The RNA samples were divided into input and acRIP. Among them, input was used to eliminate background and acRIP was performed with ac4C antibodies. The process of sequencing peak calling identifies reliable ac4C peaks and calculates FE for each ac4C peak based on the sequencing information of the two-part sample. FE, Fold Enrichment. (B and C) Venn diagrams demonstrating substantial overlap of ac4C peaks and ac4C-modified mRNAs across biological replicates in control mice. (B) Venn diagram showing the intersection of ac4C peaks among three biological replicates from hippocampal homogenates (HOM) of control mice on day 6. The numbers indicate unique and shared peaks between replicates, with 8303 peaks common to all three replicates. (C) Venn diagram showing the intersection of ac4C-modified mRNAs among the same three biological replicates, with 8107 mRNAs common to all three replicates. (D) Consensus motif analysis reveals consistent ac4C modification patterns across biological replicates in both control and memory groups. HOMER motif analysis identified the identical consensus sequence AGCAGCTG in ac4C peak regions across all biological replicates. For control mice, the motif shows highly significant p-values with target percentages at 99% confidence intervals of 57.20% (Rep 1), 54.23% (Rep 2), and 55.32% (Rep 3). For memory mice, similarly significant p-values were observed with target percentages of 56.14 (Rep 1), 54.32% (Rep 2), and 52.44% (Rep 3). The consistency of this motif across both conditions and all replicates demonstrates the specificity of ac4C modification sites. (E and F) Distribution of ac4C peak density along mRNA transcripts in control and memory groups. Metagene profiles display the relative density of ac4C peak coverage across different regions of acetylated mRNAs. Peak density distribution in HOM samples shows enrichment primarily within the CDS region, with lower density in the 5' and 3' UTRs. The analysis encompasses all three biological replicates from control (E) and memory groups (F). (G-H) Upset plots illustrating the overlap patterns of ac4C mRNAs across biological replicates. Because many genes express multiple splice isoforms, ac4C calls were summarized at the gene level (a gene is

counted as present if ≥1 isoform is ac4C-positive); isoform-specific differences between replicates may therefore not be visible at the transcript level. (G) Upset plot displaying the intersection of ac4C mRNAs among three biological replicates from control HOM samples. The analysis reveals 4494 peaks common to all three replicates, with varying numbers of peaks shared between pairs of replicates or unique to individual samples. (H) Upset plot showing the intersection of ac4C mRNAs among three biological replicates from memory HOM samples. The analysis identifies 4110 peaks common to all three replicates. The distribution patterns and overlap characteristics remain comparable between control and memory conditions, further supporting the stability of ac4C modifications after memory formation. (I) The number of ac4C peaks for each ac4C mRNA is comparable across the three biological replicates in both the HOM control and memory groups. (J) Acetylation of polyA RNA was not altered in HOM of mouse hippocampus after memory. The polyA RNA samples used for each ac4C dot-blot were 0.5 μg that falls into the linear range. The HOM polyA RNA samples of control and memory mice on day 6 after MWM training were subjected to ac4C dot-blots and methylene blue staining. Left, representative images of ac4C dot-blots and methylene blue staining; right, quantification data. n = 6 biological replicates at each condition, NS, not significant, two-tailed t-test. Data were normalized by controls. (K) Acetylation levels of ac4C mRNA were not significantly changed after memory in HOM of mouse hippocampus. Shown are cumulative distribution curves of ac4C levels for HOM in control (C) and memory (M) mice on day 6 after MWM training. The FE of ac4C mRNA was quantified in the quartile boxplots, where the solid line in the box is the median and the dashed line is the mean, where the maximum and minimum values are identified. NS, not significant, Kolmogorov-Smirnov test. FE, Fold Enrichment. (L) The normalized mRNA counts were not significantly changed in HOM of mouse hippocampus on day 6 after MWM training. Shown are cumulative distribution curves of normalized mRNA counts for HOM in C and M mice on day 6 after MWM training. The normalized mRNA counts of each group were quantified in the quartile boxplots, where the solid line in the box is the median and the dashed line

is the mean, where the maximum and minimum values are identified. NS, not significant, Kolmogorov-Smirnov test.

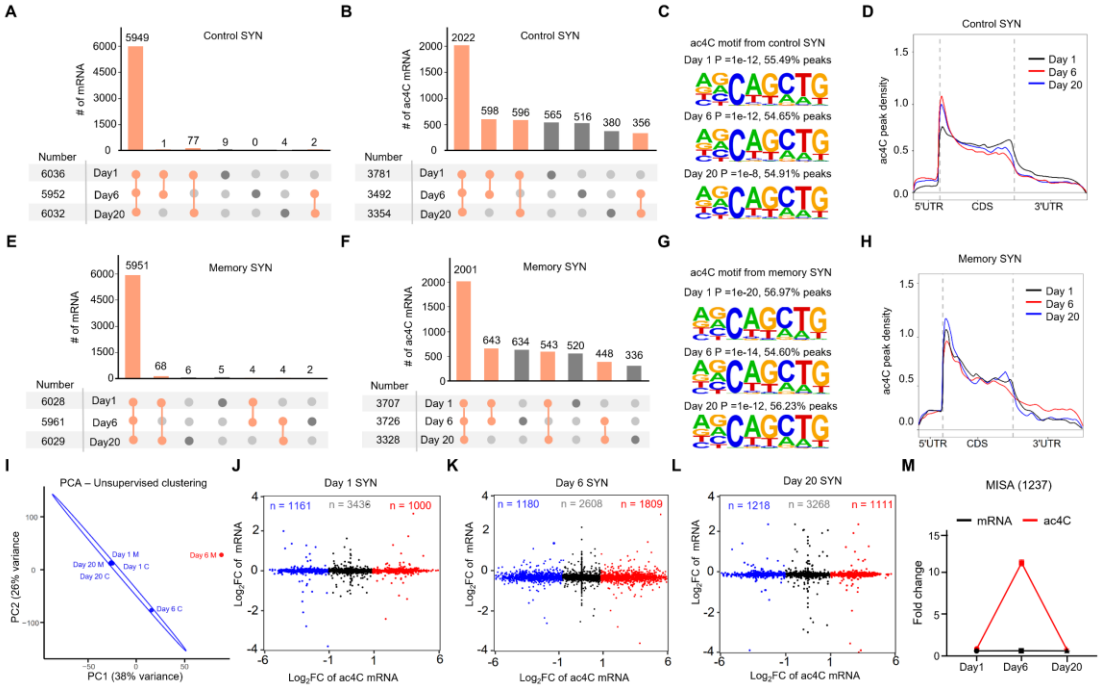

Supplementary Figure 3 Memory-induced synaptic ac4C mRNAs (MISA) in mouse hippocampus. (A-B and E-F) The transcripts and ac4C mRNAs are largely overlapping across the SYN control group (A-B) and memory group (E-F) at days 1, 6, and 20. The upset plot shows the number of mRNAs (A and E) and ac4C mRNAs (B and F) between samples. (C and G) The same consensus motif, AGCAGCTG, was identified in ac4C peak regions across the SYN control (C) and memory group (G) at days 1, 6, and 20. Consensus motif and its adjusted p-values generated by HOMER of the SYN group at days 1, 6, and 20 in acRIP-seq. (D and H) Density of ac4C peaks across different mRNA regions in the SYN control group (D) and SYN memory group (H) at days 1, 6, and 20. The line plot illustrates the density distribution of ac4C peaks in 5'UTR, CDS, and 3'UTR. The black line represents day 1, the red line represents day 6, and the blue line represents day 20. (I) PCA to demonstrate that the sample SYN memory-day6 separates from the other five samples. (J-L) Scatter plot showing the correlation between changes in mRNA expression and acetylation levels on days 1, 6, and 20. The x-axis represents the fold change in acetylation levels, while the y-axis

shows the fold change in mRNA expression. (M) The ac4C levels of MISA mRNA are upregulated following memory and return to control levels after memory retrieval. At days 1, 6, and 20, there are no significant changes in MISA mRNA levels. The black line represents the trend of mRNA expression changes, and the red line represents the trend of ac4C level changes.

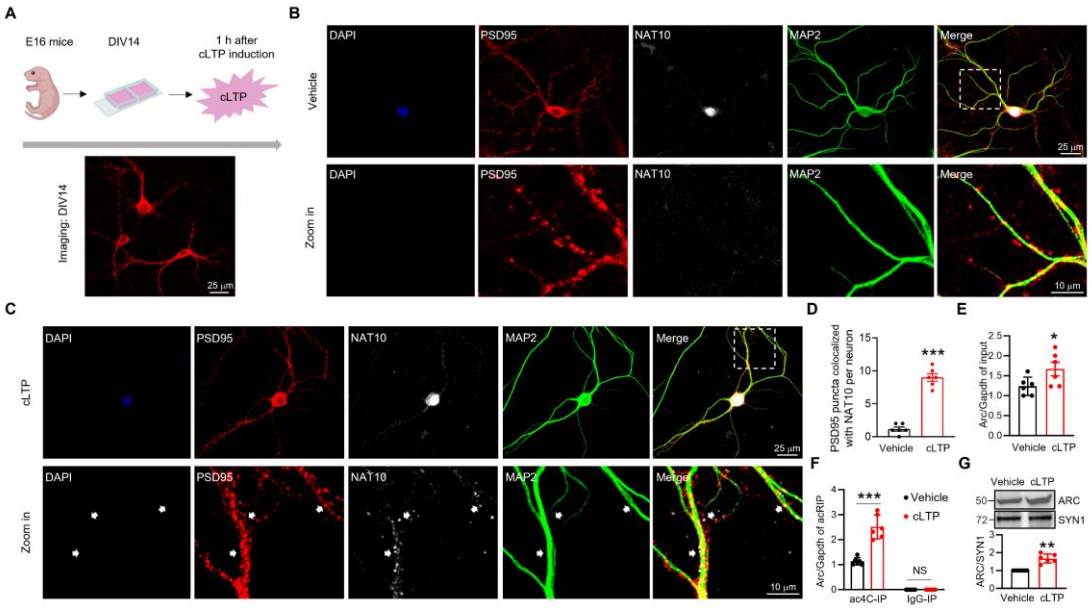

Supplementary Figure 4 Increase of NAT10 proteins and ac4C modification of Arc mRNA in the SYN of mouse hippocampal neurons and slices after cLTP stimulation. (A) Experimental design. (B and C) Distribution of NAT10 in the PSD were increased in cultured hippocampal neurons after cLTP stimulation. Shown are the fluorescent images of NAT10 were significantly increased in the PSD fraction of primary neuronal of mouse hippocampal after cLTP stimulated. Scale bar, 25 μm and 10 μm. (D) Quantification of PSD95 puncta colocalized with NAT10 per neuron. *** $P < 0.001$, two-tailed t-test. n = 6 independent experiments. (E) cLTP stimulation slightly increased Arc mRNA levels in the synaptosomes of mouse hippocampal slices. RNA purified from input samples was subjected to RT-qPCR analysis. Arc mRNA levels were normalized by Gapdh and then normalized to controls. * $P = 0.0242$, two-tailed t-test, n = 6 independent experiments. (F) ac4C modification of Arc mRNA was significantly increased after cLTP stimulation. Mouse hippocampal slices were

subjected to vehicle treatment or glycine-induced cLTP stimulation, and 1 h after that, followed by RNA purification from acRIP and IgG-IP products and RT-qPCR analysis. Data were normalized by input. *** P < 0.001, two-way-ANOVA followed by Tukey's multiple comparison test, n = 6 independent experiments. (G) cLTP increases ARC protein in synaptosomes. Quantification data for representative western blot images. ** P = 0.0011, two-tailed t-test, n = 6 independent experiments.

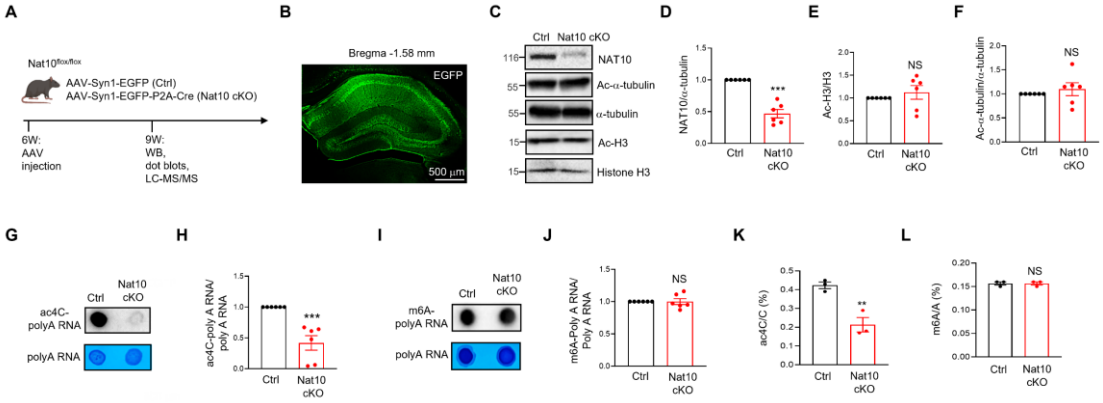

Supplementary Figure 5 NAT10-dependent ac4C modification of polyA RNA in mouse hippocampus. (A) Experimental design. Three weeks after AAV injection, Ctrl and Nat10 cKO mice underwent MWM training and probe test, followed by hippocampal tissue collection for biochemical assays. (B) Infection of AAV in the dorsal mouse hippocampus. Fluorescent images of the mouse hippocampus expressing EGFP are shown. Scale bar, 500 μm. (C) Representative western blot images. Protein samples from Ctrl and Nat10 cKO mouse hippocampus were probed with antibodies against NAT10, Ac-α-tubulin, α-tubulin, Ac-H3, and Histone H3. (D) Reduction of NAT10 protein levels in Nat10 cKO mice compared to Ctrl. Quantification data for panel C are shown. *** P < 0.001, two-tailed t-test, n = 6 biological replicates per condition, Data were normalized by controls. (E) Similar ac-H3 levels between Ctrl and Nat10 cKO mice. Quantification data for panel C are shown. NS, not significant, two-tailed t-test, n = 6 biological replicates per condition, Data were normalized by controls. (F) Similar Ac-α-tubulin levels in Ctrl and Nat10 cKO mice. Quantification data for panel C are shown. NS, not significant, two-tailed t-test, n = 6 biological replicates per condition, Data were normalized by controls. (G and H) Reduced ac4C modification of polyA RNA in the hippocampus of Nat10 cKO mice, compared with controls. The

polyA RNA samples purified from the HOM of mouse hippocampus were subjected to ac4C dot-blots and methylene blue staining. (G) Representative images. (H) Quantification data. *** $P < 0.001$, two-tailed t-test, $n = 6$ biological replicates per condition. Data were normalized by controls. (I and J) Similar m6A modification of polyA RNA in the hippocampus of control and Nat10 cKO mice. The polyA RNA samples purified from the HOM of mouse hippocampus were subjected to m6A dot-blots and methylene blue staining. (I) Representative images. (J) Quantification data. NS, not significant, two-tailed t-test, $n = 6$ biological replicates per condition. (K) Reduced ac4C modification of polyA RNA in the hippocampus of Nat10 cKO mice, compared with controls. The polyA RNA samples purified from the HOM of mouse hippocampus were subjected to LC-MS/MS analysis. The stoichiometry levels of ac4C from LC-MS/MS analysis were quantified. ** $P = 0.0077$, two-tailed t-test, $n = 3$ biological replicates per condition. (L) Similar m6A modification of polyA RNA in the hippocampus of control and Nat10 cKO mice. The polyA RNA samples purified from the HOM of mouse hippocampus were subjected to LC-MS/MS analysis. The stoichiometry levels of m6A from LC-MS/MS analysis were quantified. NS, not significant, two-tailed t-test, $n = 3$ biological replicates per condition.

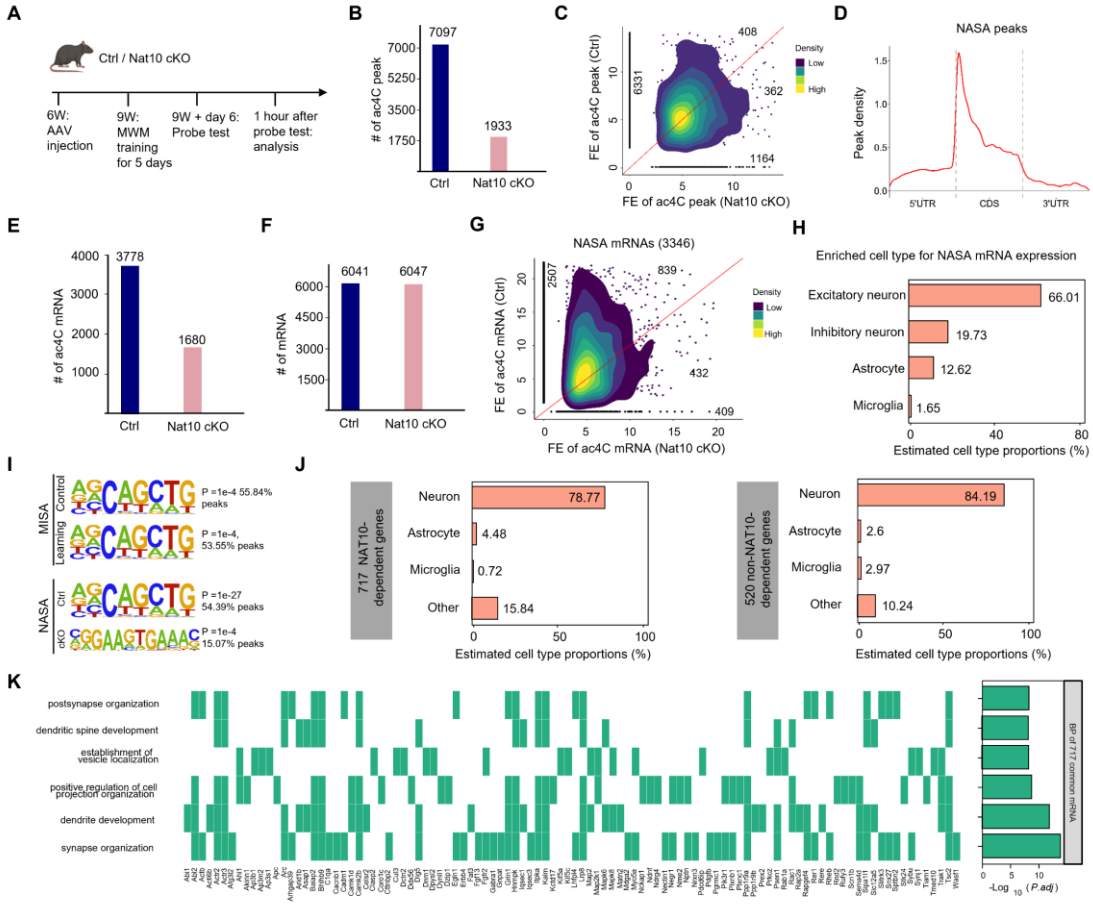

Supplementary Figure 6 NAT10-dependent of ac4C mapping in the SYN of memory mice. (A) Experimental design. Three weeks after AAV injection, the control (Ctrl) and Nat10 conditional knockout (cKO) mice were subjected to MWM training and probe test, and then the SYN fractions were purified from hippocampal tissues for low-input acRIP-seq. (B) Reduction of ac4C peak number in the SYN of Nat10 cKO mice, compared with controls. 7097 and 1933 ac4C peaks were identified in the SYN of control and Nat10 cKO mice, respectively. (C) Definition of NAT10-dependent ac4C peaks through acRIP summits displaying higher FE values in control relative to Nat10 cKO mice. Shown are the density scatter plot of ac4C peaks. Each dot represents an ac4C peak. 6331 ac4C peaks are specifically identified in the SYN of control but not Nat10 cKO mice. The FE of 408 ac4C peaks was higher in the SYN of control mice than Nat10 cKO mice. (D) NAT10-dependent ac4C peaks are predominantly located in the CDS region of mRNA. The plot shows the density of ac4C peaks along various mRNA regions, including the 5'UTR, CDS, and 3'UTR. (E) Reduction of ac4C mRNA

number in the SYN of Nat10 cKO mice, compared with controls. 3778 and 1680 ac4C mRNAs were identified in the SYN of control and Nat10 cKO groups, respectively. (F) Similar mRNA numbers identified in the SYN of control and Nat10 cKO mice. 6041 and 6047 mRNAs were identified in the SYN of control and Nat10 cKO mice, respectively. (G) Definition of NAT10-dependent synaptic ac4C (NASA) mRNA through acRIP summits displaying higher FE values in control relative to Nat10 cKO mice. Shown are the density scatter plot of ac4C mRNA. Each dot represents an ac4C mRNA. 2507 ac4C mRNAs are specifically identified in the SYN of control but not Nat10 cKO mice. The FE of 839 ac4C mRNA was higher in the SYN of control mice than Nat10 cKO mice. (H) The expression of NASA mRNA is mostly enriched in excitatory neurons of mouse hippocampus. Shown are the percentage of NASA mRNA whose expression was relatively enriched in different cell types of mouse hippocampus through analysis of the single-cell RNA-sequencing dataset (http://dropviz.org). (I) A shared consensus motif, AGCAGCTG, was consistently enriched within ac4C peak regions in both the MISA and NASA groups, as identified by HOMER from acRIP-seq data. Notably, in Nat10 cKO samples, the ac4C-associated motifs exhibited a marked loss of the CXX sequence feature, suggesting that Nat10 depletion alters the sequence preference for ac4C deposition. (J) Analysis of the cell-type enrichment using the method of CIBERSORT reveals that both Nat10-dependent and independent MISA mRNAs are highly expressed in neurons. (K) Gene Ontology BPs associated with the 717 common mRNAs from Figure 6D are significantly enriched. The x-axis indicates both the included mRNAs and the negative logarithm of the adjusted p-values, representing enrichment significance, while the y-axis displays the corresponding biological processes.

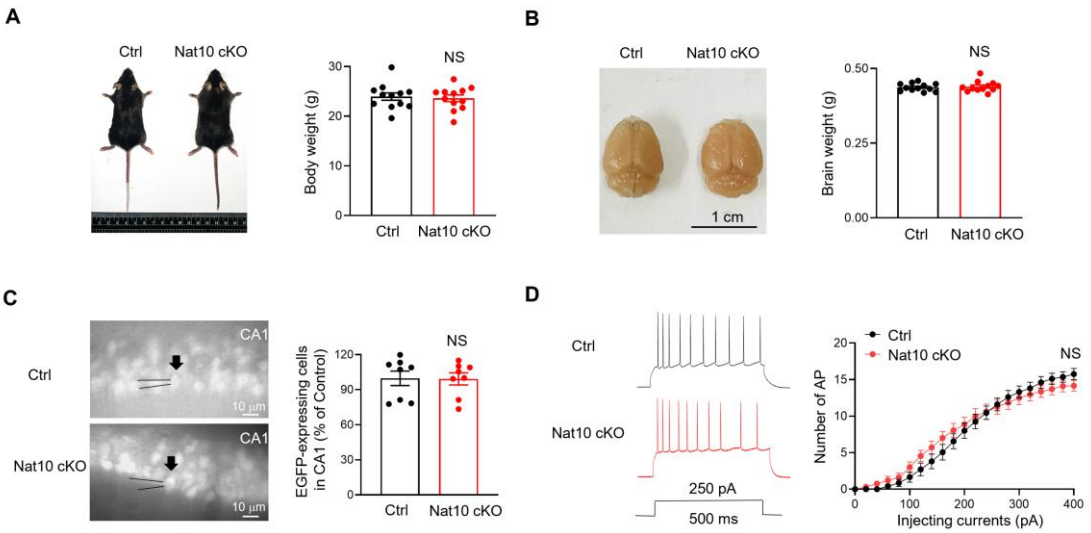

Supplementary Figure 7 Downregulation of NAT10 in mouse hippocampus does not affect body or brain weight, neuronal number or intrinsic excitability. (A) Similar body weight between 10-week-old Ctrl and Nat10 cKO mice. Left, representative images of the mice, right, quantification of body weight. n = 12 mice for each group, NS, not significant, two-tailed t-test. (B) Similar brain weight between 10-week-old Ctrl and Nat10 cKO mice. Left, representative images of mouse brain, right, quantification of brain weight. n = 12 mice for each group, NS, not significant, two-tailed t-test. (C) Similar number of neurons expressing EGFP in the CA1 region of 10-week-old Ctrl and Nat10 cKO mice. Left, representative images of CA1 neurons expressing EGFP, right, quantification of EGFP-expressing cells in CA1 region. n = 8 slices from 4 mice, NS, not significant, two-tailed t-test. Data were normalized by Ctrl. (D) Similar intrinsic excitability of CA1 pyramidal neurons between 10-week-old Ctrl and Nat10 cKO mice. Left, representative traces of action potentials (AP) of CA1 pyramidal neurons; right, quantification of AP number after injection of different currents into CA1 pyramidal neurons. n = 20 cells from 4 mice per group, NS, not significant, two-way ANOVA followed by Sidak's multiple comparison test.

Supplementary Tables

Supplementary Table 1. Library Information of acRIP-seq.

Supplementary Table 2. List of mRNAs identified by regular acRIP-seq (HOM).

Supplementary Table 3. List of mRNAs identified by low-input acRIP-seq (SYN).

1963 Supplementary Table 4. The information of MISA mRNA.

1964 Supplementary Table 5. The information of NASA mRNA.